Amphibole-bearing Multiphase Solid Inclusions in Olivine and Plagioclase from a Layered Gabbro : Origin of the Trapped Melts

Hoshide, Takashi
Department of Earth and Planetary Sciences, Faculty of Sciences, Kyushu University

Obata, Masaaki
Department of Geology and Mineralogy, Graduate School of Science, Kyoto University

出版情報：Journal of Petrology. 53 (3), pp.1-31, 2012-01. Oxford University Press
バージョン：

JOURNAL OF PETROLOGY | VOLUME 53 | NUMBER 2 | PAGES 1–31 | 2012 | doi:10.1093/petrology/egr067
Journal of Petrology Advance Access published January 12, 2012

Amphibole-bearing Multiphase Solid Inclusions in Olivine and Plagioclase from a Layered Gabbro: Origin of the Trapped Melts

TAKASHI HOSHIDE[1,2]* AND MASAAKI OBATA[1]

[1]DIVISION OF EARTH AND PLANETARY SCIENCES, DEPARTMENT OF GEOLOGY AND MINERALOGY, GRADUATE SCHOOL OF SCIENCE, KYOTO UNIVERSITY, KYOTO 606-8502, JAPAN

[2]DEPARTMENT OF EARTH AND PLANETARY SCIENCES, FACULTY OF SCIENCES, KYUSHU UNIVERSITY, 6-10-1 HAKOZAKI, HIGASHI-KU, FUKUOKA 812-8581, JAPAN

RECEIVED SEPTEMBER 16, 2009; ACCEPTED NOVEMBER 15, 2011

This study presents new data regarding the petrographic and mineralogical characteristics of amphibole-bearing multiphase solid inclusions (MSI) enclosed in olivine and plagioclase from a well-characterized Japanese layered gabbro, the Murotomisaki Gabbroic Intrusion. Bulk compositions of the MSI were obtained using wavelength-dispersive (WDS) and energy-dispersive (EDS) techniques combined with modal analysis. Many MSI in olivines are spherical or polygonal in shape and are mainly composed of pargasitic amphibole, orthopyroxene, and mica (biotite and aspidolite). The MSI in olivine phenocrysts in the chilled margins of the intrusion are composed of plagioclase and hornblende rather than pargasite. Many of them are found to be enriched in olivine components in their bulk compositions, and therefore they cannot be regarded as simple trapped basaltic melts or their derivatives. The MSI in plagioclase are more irregular in shape and occur in the resorbed part of calcic plagioclase cores; they are mainly composed of pargasite and sodic plagioclase. Attempts were made to obtain the original composition of the MSI melts by applying a correction for Fe–Mg exchange reactions with the host olivine. It was found that after the correction, the MSI in the chilled margin were closest to the published initial basaltic melt composition, whereas the olivine-hosted MSI from the olivine gabbros were still fairly high in olivine components despite the correction. Such post-entrapment modification was probably minimal for the plagioclase-hosted MSI because plagioclase is essentially free of Mg and Fe, and therefore plagioclase-hosted MSI are believed to represent the compositions of the original trapped melts. These are characteristically enriched in plagioclase components. We believe that the anomalous compositions of the trapped melts (after the corrections) were generated by local dissolution of olivine and plagioclase caused by the introduction of water from lower horizons of the crystallization boundary layer in a magma chamber. The MSI are therefore considered to provide new evidence for the dissolution of silicates by hydrous fluxing in a lower crystallizing boundary layer of a magma reservoir during solidification of basaltic magma.

KEY WORDS: *crystallized melt inclusion; amphibole; magmatic differentiation; water; fluid; boundary layer; magma chamber*

INTRODUCTION

The study of melt inclusions in igneous rocks is important because it provides potentially useful information about the nature of the primary melt and its subsequent fractionation trend. Significant advances have been made in the study of melt inclusions in volcanic rocks over the last four decades, which have contributed to our understanding of the petrogenesis of the parental magmas (Sobolev & Shimizu, 1993; Kamenetsky *et al.*, 1997; Berry *et al.*, 2008; Trua *et al.*, 2010), in particular, the presence and composition of volatile components (Anderson, 1973; Lowenstern, 2003; Saito *et al.*, 2010). Unlike volcanic rocks, however, 'melt inclusions' in plutonic rocks are more difficult to

*Corresponding author. Present address: Department of Earth and Planetary Sciences, Faculty of Sciences, Kyushu University, 6-10-1 Hakozaki, Higashi-ku, Fukuoka 812-8581, Japan.
E-mail: hoshide.takashi.180@m.kyushu-u.ac.jp

study because they have not been 'quenched' and typically occur as multiphase solid inclusions (MSI). The MSI do not necessarily represent the frozen melt in terms of their bulk composition and may have been substantially modified from the original trapped melts, during or after crystallization, by reaction with their hosts (and possibly with the surrounding melt outside the host) (Danyushevsky *et al.*, 2000; Gaetani & Watson, 2000; Veksler, 2006; Jakobsen *et al.*, 2011). Thus, we must first identify these MSI as frozen melts and then make the appropriate corrections to the analytical data to retrieve the primary composition of the melts at the time of their entrapment.

During the course of petrological investigations of a Japanese layered gabbro, the Murotomisaki Gabbroic Intrusion (MGI) (e.g. Hoshide *et al.*, 2006), we noted that there were many MSI enclosed in olivine and plagioclase. Based on analyses of their bulk composition, it soon became apparent that these MSI, particularly those in olivine, had rather anomalous compositions, enriched in olivine components, that could not be produced by normal crystal fractionation processes from a basaltic magma. The purpose of this study is to present new data for these MSI from well-characterized sections of the intrusion as a function of their stratigraphic position and to discuss their origin. Bulk compositions of MSI were obtained from a combination of mineral modal and electron microprobe analyses. Special attention was paid to the compositional zoning of the minerals within the MSI because it might provide useful information on the mode and the conditions of crystallization differentiation of the trapped melts. The hypothesis we propose for the origin of the anomalous melts involves local dissolution of the olivine and plagioclase primocrysts during the solidification of the intruded magma body as a whole, induced by fluxing of H_2O-rich fluids that were liberated and supplied from crystallizing magma in the lower magmatic boundary layer. This may have significant implications for the origin of igneous layering and the formation of pegmatitic structures, as described below.

MUROTOMISAKI GABBROIC INTRUSION

The Murotomisaki Gabbroic Intrusion (MGI) is a sill-like layered intrusion (up to *c.* 210 m thick) of tholeiitic affinity (Yajima, 1972) located near Cape Murotomisaki, Shikoku, Japan (Fig. 1). It has been shown that the intrusion was differentiated from a single batch of basaltic magma emplaced into Tertiary sediments (the Shimanto Formation) at *c.* 14 Ma (Hamamoto & Sakai, 1987). The intrusion is subdivided into three major stratigraphic zones on the basis of the cumulus phases and grain size: a Lower Zone (LZ), a Middle Zone (MZ), and an Upper Zone (UZ) (Fig. 2a). A brief summary of the characteristics of each zone is given below. For further petrographic details the reader is referred to Hoshide *et al.* (2006) and Hoshide & Obata (2009).

The Lower Zone

This occupies the lower half of the intrusion and consists of fine- to medium-grained olivine gabbro. Olivine and plagioclase are the only cumulus phases and augite occurs only interstitially although it dominates in volume in some samples. Amphibole occurs in subordinate amounts overgrowing the interstitial augite (Fig. 3d). Olivine near such amphiboles often has reaction rims of orthopyroxene, which is partly altered to talc (Fig. 3d).

The Lower Zone has a chilled margin of *c.* 3 m thickness at its base where the rock texture varies from fine-grained basaltic in the lowermost part to doleritic in the upper part. The finest-grained part, restricted to a few centimetres from the lower contact, contains a few microphenocrysts of olivine (up to 8 vol. %, average grain size 250 μm) and plagioclase (~1–3 vol. %, average grain size 200–300 μm) set in a dark-colored, fine-grained matrix that is composed of olivine, plagioclase (<50 μm), pyroxene, hornblende, and opaque phases. The phenocrystic olivine shows clear normal zoning from Fo_{83} in the core to Fo_{65} in the rim. The composition of olivine (Fo_{83}) in the core is the most magnesian throughout the intrusion.

Apart from the chilled margin, the Lower Zone is further subdivided into two subzones: a crystal accumulation (AC) subzone (lower 40 m) and a crystal growth (GR) subzone (upper 60 m) (Fig. 2a). The AC subzone is defined by its higher crystal number densities of olivine above the average value of the whole intrusion, which is in accord with the value of the lower chilled margin (Fig. 2d), whereas the GR subzone has reduced crystal number densities of olivine below the average value (Hoshide *et al.*, 2006). The olivine grain size is relatively constant in the AC subzone and rapidly increases in the GR subzone (Fig. 2c). The plagioclase grain size, however, gradually and monotonically increases (up to 10 mm in length) from the lower chilled margin even within the AC subzone (not shown in Fig. 2). There is one clear peak of olivine modal abundance in the AC Zone (Ol), which coincides with that of olivine crystal number density, whereas two other peaks of olivine abundance occur in the GR subzone (O2 and O3), each of which may be correlated with peaks in olivine grain size (Fig. 2c). The AC subzone looks homogeneous and monotonous in the field except for some gradual upward coarsening of the rocks. The GR subzone, on the other hand, is more inhomogeneous and contains conspicuous compositional banding or layering as well as abundant pods and veins of gabbroic pegmatite (a few centimetres to 2 m in thickness) and layers of anorthosite (Hoshide & Obata, 2009).

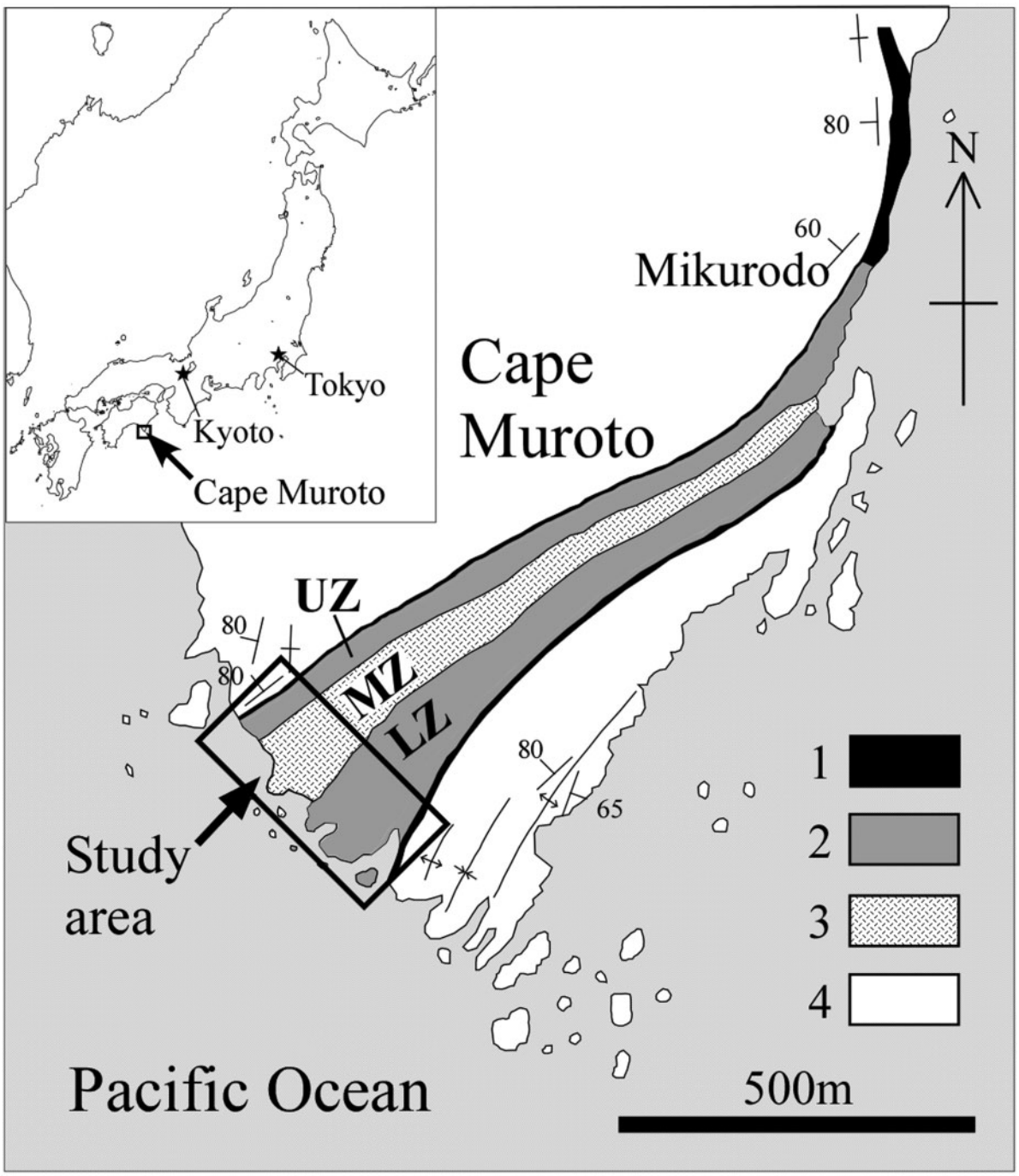

Fig. 1. Simplified geological map of the Murotomisaki Gabbroic Intrusion. Modified from Hoshide *et al.* (2006). 1, chilled marginal zone; 2, olivine gabbro; 3, coarse gabbro; 4, country rocks (sandstone–shale alternation). LZ, Lower Zone; MZ, Middle Zone; UZ, Upper Zone.

The Middle Zone

This is composed of coarse gabbros comprising augite and plagioclase. These have been divided into types I and II based upon their cumulus phases and rock textures (Akatsuka *et al.*, 1999; Hoshide *et al.*, 2006). Type I contains only one cumulus phase, plagioclase (average grain size 1–2 cm), set in a matrix of augite, forming an ophitic texture. This occurs in the upper Middle Zone about 130 m above the base. Type II gabbro contains augite (average grain size 1–2 cm) and plagioclase (average grain size ~1 cm) as cumulus phases and occurs in the lower half of the Middle Zone. Augite is more abundant in Type II

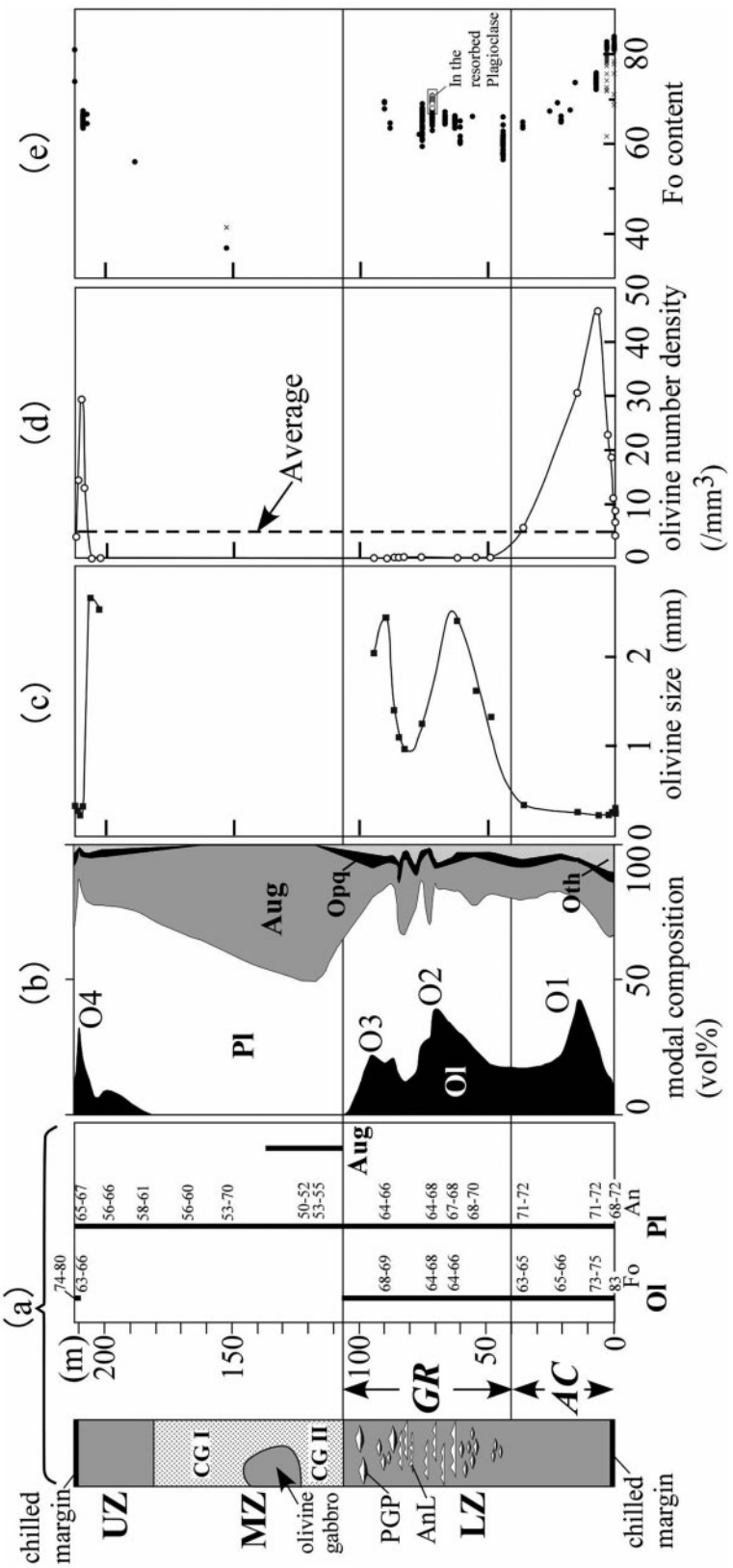

Fig. 2. Lithological and compositional variations in the Murotomisaki Gabbroic Intrusion. (a) A schematic lithological column (left) and cumulus phases with their approximate compositions (i.e. Fo and An contents) (right); (b) modal compositions; (c) average crystal size of olivine; (d) crystal number density of olivine; (e) Fo content of olivine (filled circles, cores; crosses, rims) from Hoshide & Obata (2009). The dashed line in (d) shows the average (and initial) value of the crystal number density of olivine throughout the intrusion. LZ, Lower Zone; MZ, Middle Zone; UZ, Upper Zone. CG I and II, coarse gabbro (type I and II, respectively). AC, AC subzone; GR, GR subzone. PGP, podiform gabbroic pegmatite; AnL, anorthositic layer. Pl, plagioclase; Ol, olivine; Aug, augite; Opq, opaque minerals; Oth, other phases (including hypersthene, hornblende, biotite and chlorite). Hornblende-rich samples from the Upper Zone (see Petrography section) are very local and thus are omitted from this diagram. Ol, O2 and O3 indicate three peaks of olivine abundances.

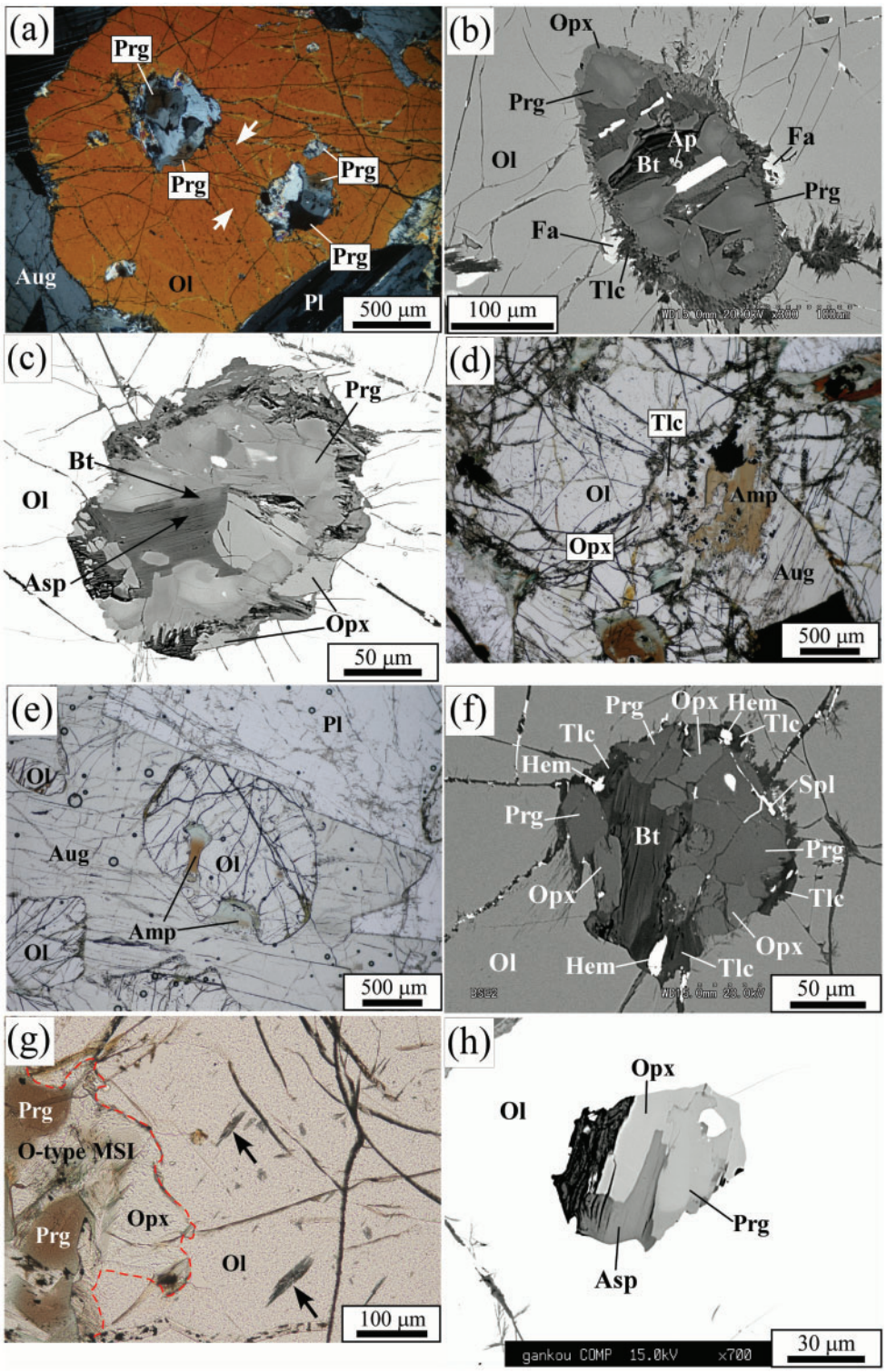

Fig. 3. Photomicrographs of O-type MSI and other related textures from the Lower Zone of the MGI. (a) An olivine crystal containing O-type MSI, from an olivine-rich layer (43 m from the base). [Note that brownish cores of pargasite (Prg) are located closer to the olivine wall.] Thin platelets of augite–magnetite symplectite (shown with white arrows) occur in the olivine. Cross-polarized light. (b) Back-scattered electron (BSE) image of an O-type MSI (in olivine) from sample 92080704 (70 m from the base). Orthopyroxene occurs in the outermost rim of the MSI, adjacent to the olivine wall. (Note that some pargasite crystals have crystal facets facing inward into the MSI.) Some orthopyroxene has been altered to talc, adjacent to which distinctively Fe-rich olivine (Fa, ~Fo_{34}) occurs in the olivine wall. (c) BSE image of an O-type MSI

(continued)

than in Type I. Hornblende, biotite, apatite, and titaniferous magnetite are common accessory phases in both types (Fig. 2b). Olivine does not occur as a cumulus phase in either type, but does occur rarely interstitially (size 0·5–1 cm) in one sample of Type I gabbro (sample 91080906); its composition is $Fo_{37–40}$, which is the most iron-rich olivine throughout the intrusion.

The Upper Zone

This is nearly a mirror image of the Lower Zone except for its smaller thickness than the Lower Zone. It is composed of fine- to medium-grained olivine gabbro and has a chilled margin of *c.* 2 m thickness at its top. The upper chilled margin, however, is more coarse-grained than the lower one, and lacks the very fine-grained selvedge (of basaltic texture) observed in the lower chilled margin. Moving downward from the upper contact, the fine-grained doleritic margin grades into medium-grained picritic gabbro (with plagioclase grain size of *c.* 2 mm in length) where olivine is the most abundant and highest in crystal number density in the Upper Zone (Fig. 2). Below this horizon, plagioclase is the only cumulus phase and olivine occurs only interstitially (i.e. as a postcumulus phase). Olivine gabbros in a distinct horizon (~208 m from the base) in the Upper Zone contain many small spherical clots of 1–3 mm in size that are composed of polycrystalline greenish hornblende (the modal composition of this part is not shown in Fig. 2b). The olivine composition in the Upper Zone varies in the range of $Fo_{80–55}$ with a general tendency to become more iron-rich downward (Fig. 2e).

MULTIPHASE SOLID INCLUSIONS

Three types of inclusion

Multiphase solid inclusions (MSI) exclusively occur in the cumulus crystals of olivine and plagioclase in the Murotomisaki Gabbroic Intrusion. Although the mineralogical and textural characteristics of the MSI are variable, reflecting their host phase and their stratigraphic position, amphibole (pargasitic hornblende to hornblende) is a common and dominant phase. For this reason the MSI, particularly those in olivine, were once referred to as 'amphibole clots' (e.g. Hoshide & Obata, 2009). For ease of description, we first classify the inclusions into two major categories: O-type, for those hosted in olivine, and P-type, for those hosted in plagioclase. The O-type MSI are composed mainly of pargasitic amphibole, orthopyroxene, and mica. In addition, because of their mineralogically and compositionally distinct nature, we define a third type, the O'-type, for those hosted in olivine phenocrysts in the lower chilled margin. The O'-type MSI are, in contrast to the O-type, composed of hornblende (not pargasite), plagioclase, and orthopyroxene, and have a different bulk composition from the O-type MSI as shown below. All types of MSI are holocrystalline with no glass. Other kinds of multiphase solid inclusion also occur occasionally in some apatite and ilmenite. However, because of their rarity, we do not discuss them further here.

Petrography of the MSI

The mineralogical characteristics and approximate modal composition of each type of MSI are summarized in Table 1 and are described below.

O-type MSI

These are typically round or sometimes nearly polygonal in shape, varying in size from several tens to several hundred micrometres in diameter; some are elongated in shape (Figs 3a and 4). The size of the MSI is variable, even within a single thin section. Although some inclusions, particularly the large ones, may be partly connected in three dimensions to the outer matrix of the host olivine crystals, most MSI are considered to be 'true inclusions' in the sense that they are completely enclosed in the host, and disconnected from the matrix. The O-type MSI are modally dominated by pargasitic hornblende and orthopyroxene with subordinate amounts of biotite-like mica. Common accessory phases include apatite, titanomagnetite, hematite, and sulfides. Olivine is absent in this type of MSI except for rare, tiny inclusions in some pargasite crystals. Plagioclase is also absent in this type. Within the Lower Zone, amphibole is the dominant phase in the GR subzone, whereas orthopyroxene is more dominant in the AC subzone, except in the olivine-rich horizon (Ol). Figure 5 shows the stratigraphic variation in the abundance and average size of the O-type MSI, which shows that they are larger and more abundant in the GR subzone than in the AC subzone. In more detail, as we move upwards from the olivine-rich horizon in the AC subzone (peak Ol), the abundance of the O-type MSI first

Fig. 3 Continued
including a composite grain of K-rich mica (biotite) and Na-rich mica (aspidolite; Asp). From sample 92080706 (71 m from the base). (d) Hornblende occurs in the matrix, at the edge of an interstitial augite grain. From sample 91080708 (62 m from the base). Olivine near the hornblende often has a rim of orthopyroxene, which is now altered to talc. Plane-polarized light. (e) 'Matrix' hornblende also occurs in an embayment in an olivine crystal, which is itself included in a large augite crystal. Plane-polarized light. From sample 06080701 (50 m from the base). (f) BSE image of an O-type MSI (in olivine) from the upper part of the AC subzone (sample 92080912; 21 m from the base). (g) Thin oriented platelets of augite–magnetite symplectite lamellae in olivine near an O-type MSI (indicated by arrows). Plane-polarized light. (h) BSE image of an O-type MSI including aspidolite.

Table 1: Mineralogical characteristics of three types of MSI from MGI

Inclusion	Host zones	Main constituent phases		Accessory phases	Remarks
Size range (μm)		Phase	Modal (vol. %)		
O-type; host phase Ol					
30–600	AC (lower part) and GR	Amp	41–64	Cpx, Ap, Ti-Mag, sulfide	Amp, strongly zoned; Pl rare
		Opx	29–39		
		Mica*	6–19		
	AC (upper part)	Amp	30–33	Ap, Ti-Mag, sulfide	Amp, moderately zoned
		Opx	44–45		
		Mica*	23–24		
O′-type, host phase Ol (phenocryst)					
10–100	lower chilled margin	Amp	48		voids abundant
		Pl	37		
		Opx	4		
P-type, host phase Pl					
100–1000	GR†	Amp	13–41	Ilm, sulfide	Pl zoned An_{43-60};
		Pl	45–82		Ol rare
		Ti-Mag	2–7		insubstantial void
		Ap	2–6		

*Mica includes biotite, aspidorite and chlorite.
†P-type MSI are distributed in all of the zones, but the features described here apply only to those from the GR subzone. Amp, amphibole; Opx, orthopyroxene; Cpx, clinopyroxene; Ap, apatite; Ti-Mag, titaniferous magnetite; Ilm, ilmenite. Other abbreviations are the same as in Fig. 2.

Fig. 4. Distribution of O-type MSI in olivines in an olivine gabbro (from the GR subzone, sample 92080704, 70 m from the base). The MSI are highlighted white and outlined on a thin section photomicrograph, taken in plane-polarized light.

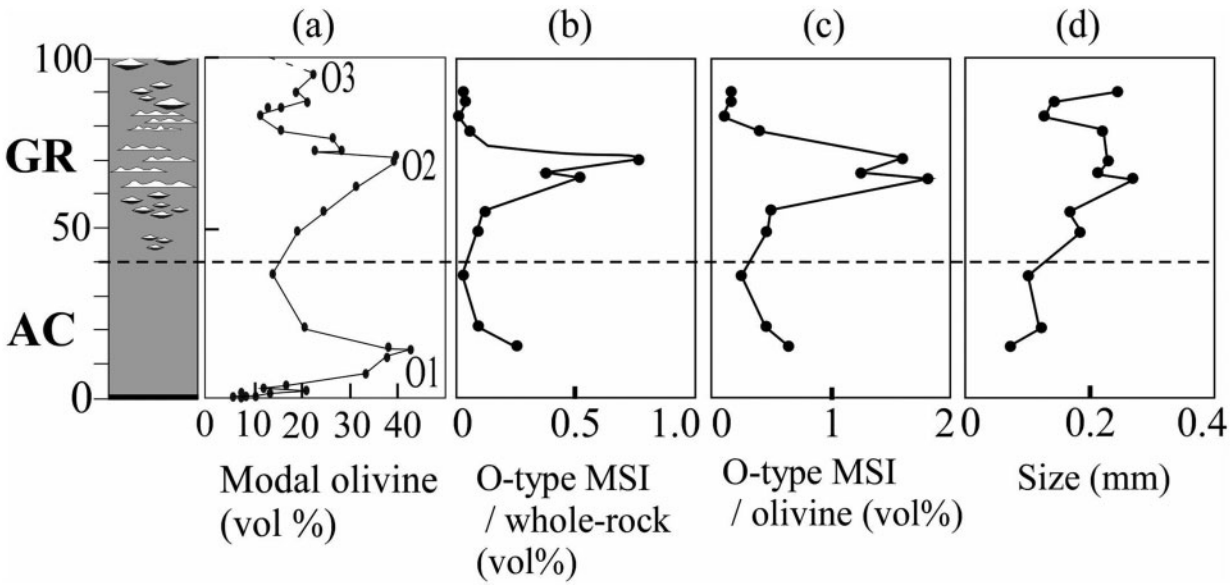

Fig. 5. Stratigraphic variations of (a) the abundance of olivine (vol. %), (b) modal variation of O-type MSI, (c) modal variation of O-type MSI normalized by the modal olivine, and (d) average size of O-type MSI. Approximate horizon of the AC–GR boundary is indicated by the dashed line.

decreases before increasing rapidly in the GR subzone towards the olivine-rich horizon (peak O2), after which it decreases again (Fig. 5b). This modal variation is shown also in the olivine-normalized mode (i.e. mode of the inclusion divided by the modal proportion of olivine) (Fig. 5c), which indicates that the increase in inclusion abundance cannot be ascribed to the accumulation of the olivine crystals. The O-type MSI in the Upper Zone are mineralogically similar to those from the Lower Zone AC subzone but are less abundant (not shown in Fig. 5).

The O-type MSI have a concentric internal structure with orthopyroxene occupying the outermost part in contact with the olivine host (Fig. 3b and c) surrounding amphibole with mica at the center. Talc occurs locally, replacing the orthopyroxene, and is associated with irregularly shaped, small grains of hematite (Fig. 3b). The boundary between the talc and the orthopyroxene is irregular. The olivine wall in direct contact with the talc is distinctly more Fe-rich than the adjacent host olivine (Fig. 3b).

The amphiboles are typically zoned, containing a brownish core of strongly pargasitic composition mantled by a greenish rim of pargasite to hornblende. The zoning pattern is not symmetrically concentric, and the pargasitic core is displaced closer to the olivine wall (Fig. 3a), which may suggest that pargasitic amphibole first nucleated on the olivine wall (or the orthopyroxene rim) and grew inward into the inclusion. In the orthopyroxene-dominant varieties (i.e. those from the upper part of the AC subzone), the amphibole does not show such distinct zoning and does not contain the strongly pargasitic cores (Fig. 3f). Some pargasitic cores contain small blebs of augite (~10 μm in diameter). These augite inclusions share the same extinction angle within a restricted area of the host amphibole, which suggests that they were originally part of the same grain. Furthermore, some amphiboles contain minute, fluid-like inclusions (less than 10 μm in size). Cummingtonite occurs locally, and is probably of a secondary origin.

The biotite-like micas from the inner portion of the O-type MSI (Fig. 3b, c and f) are optically inhomogeneous, some being pale green in plane-polarized light and others pale brown. Locally, some of the micas have been partly or completely altered to chlorite. Microprobe analysis reveals that many of the biotite-like micas are not really biotite and that some are the Na-bearing mica aspidolite, as described below.

The amphibole in some 'imperfect' MSI partly enclosed in olivine that is further included in a large augite crystal (Fig. 3e) is not pargasitic but hornblende like that in the matrix. It seems, therefore, that the fact that the amphibole is pargasitic can be an assurance that the inclusions are perfect and that true inclusions are physically and chemically separate from the matrix.

O'-type MSI

These are smaller in size (10–100 μm) than the O-type (Fig. 6a). Unlike the O-type MSI, plagioclase is an essential daughter phase, as well as amphibole and

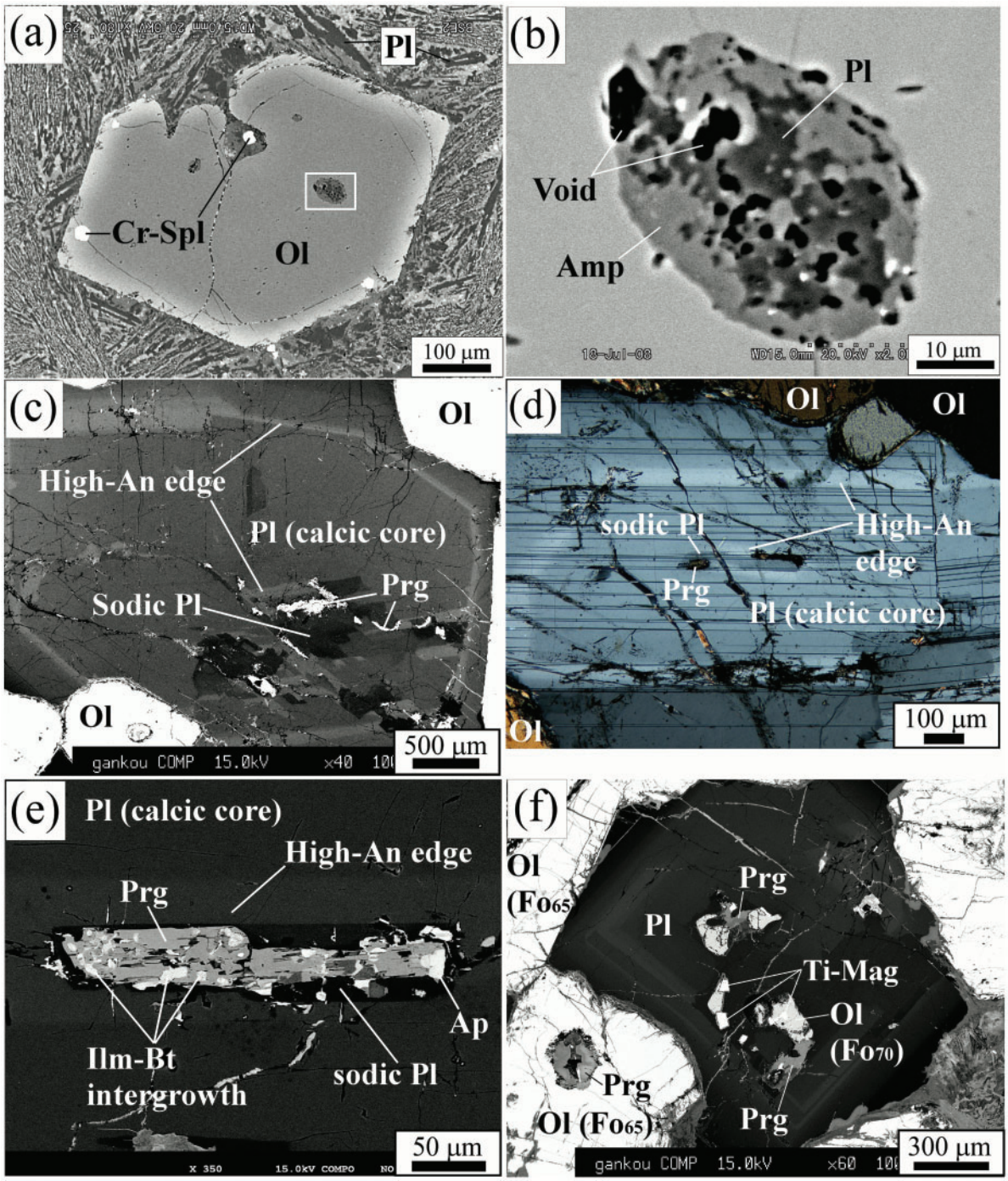

Fig. 6. Photomicrographs of O'-type and P-type MSI. (a) Back-scattered electron (BSE) image of a phenocrystic olivine containing O'-type MSI. Sample from the lower chilled margin (sample LCM32). (Note that one MSI is connected to the matrix forming a 'bottle-neck' structure.) (b) A close-up image of one of the MSI indicated by the frame in (a). (c) BSE image of P-type MSI occurring in an embayment in the calcic core of a zoned plagioclase, from GR subzone (sample 92080706; 71 m from the base). High-An edges occur around the P-type MSI. (d) A photomicrograph of a P-type MSI in a pool in a plagioclase core (from the GR subzone). From sample 92080706 (71 m from the base). (e) BSE image of a P-type MSI, from the GR subzone (sample 91080509; 55 m from the base). Submicron-scale intergrowths of ilmenite and chlorite occur in pargasitic amphibole. (Note the high-An rim around the P-type MSI.) (f) BSE image of assemblies of small crystals of magnesian olivine (Fo_{70}) and magnetite occurring in embayments in the calcic core of a zoned plagioclase. From sample 92080706 (71 m from the base). Ti-Mag, titaniferous magnetite. Other abbreviations for minerals are the same as in Figs 2 and 3.

orthopyroxene (Table 1, Fig. 6b). The plagioclase is fairly sodic, $An_{30–50}$ (Table 6). The amphibole in this type is hornblende in composition and not pargasite. Voids (or vesicles) are abundant, which suggests that the melts were saturated with volatiles in this type when they were entrapped. Like the O-type MSI, orthopyroxene and amphibole tend to occupy the outer parts of the MSI, whereas plagioclase tends to occur inside (Fig. 6b). Rarely this type of MSI is connected to the surrounding matrix via cuspate olivine boundaries (Fig. 6a), showing how the ambient melt may be entrained in a growing crystal of olivine to form this type of MSI. In some chilled margin dolerites, both O-type and O'-type MSI occur together in the same crystals of olivine.

P-type MSI

These are more ubiquitous and occur in plagioclase throughout the intrusion, except for the chilled margins. They are more irregular in shape than the O- and O'-type. The P-type MSI are particularly abundant in the GR subzone. They are composed of pargasitic amphibole and sodic plagioclase with accessory titaniferous magnetite. They typically occur in embayments (Fig. 6c) or in pools in the calcic cores of zoned plagioclase (Fig. 6d). Thin, high-An rims (Hoshide & Obata, 2009), which are more calcic in composition than the cores, are developed surrounding the core and are not counted as a part of the MSI (Figs. 6c–e). The daughter phases of the P-type MSI in the GR subzone are sodic plagioclase ($An_{43–60}$) and pargasite with accessory apatite, titaniferous magnetite, ilmenite, and sulfides (e.g. $CuFeS_2$). Pargasite always occurs adjacent to the inclusion wall (Fig. 6d). Titaniferous magnetite has been altered to an intergrowth of magnetite and ilmenite. Where titaniferous magnetite is included in pargasite, the magnetite intergrowth appears to have been replaced by biotite, but the ilmenite lamellae survive the alteration (Fig. 6e; Ilm–Bt intergrowth). The apatite often contains tiny fluid-like inclusions (<10 μm). Olivine is typically absent in the P-type MSI, but the sodic plagioclase portion rarely does include assemblages of small amoeboidal crystals of olivine (~Fo_{70}; much more magnesian than ordinary olivines outside the plagioclase) and magnetite (Fig. 6f).

SAMPLES AND ANALYTICAL METHODS

Sample selection and measurement of abundances and sizes of MSI

For a detailed study of the MSI, we selected 18 samples from different horizons of the intrusion (six from the AC subzone and 12 from the GR subzone) from the 100 m thick Lower Zone (Fig. 2a). The abundance and average size of the olivine-hosted MSI was measured for 12 selected samples (Fig. 5). Eight samples were selected for microprobe analyses of the minerals of the MSI, the host olivine, and the surrounding matrix. Among them, the bulk compositions of the olivine-hosted MSI were obtained for five samples (three from the AC subzone and two from the GR subzone). Two samples from the GR subzone were used for the analysis of the bulk compositions of the P-type MSI.

Electron microprobe analysis

Backscattered electron images, X-ray mapping, and quantitative analyses of minerals were obtained using a JEOL WDS electron microprobe JXA-8105 installed at Kyoto University. X-ray elemental maps were acquired at 15 kV accelerating voltage, 500–600 nA beam current, 1 μm beam diameter, and a count time of 400 ms per pixel. For quantitative analyses, an accelerating voltage of 15 kV and a beam current of 10 nA were used throughout; each element was counted for 10 s except for the halogens. Cl and F in amphibole and mica were counted for 90 s for each element. Natural and synthetic minerals of well-known compositions were used as standards: quartz (Si), rutile (Ti), corundum (Al), chromium oxide (Cr), hematite (Fe), rhodonite (Mn), periclase (Mg), wollastonite (Ca), NiO (Ni), albite (Na), sanidine (K), fluorite (F) and tugtupite (Cl). Beam sizes of 3 μm in diameter were used for quantitative analyses. Cl and F volatility and Na loss under the electron beam were monitored using a Chart Recorder utility and kept to a minimum during electron microprobe analyses. A ZAF correction was employed for all the analyses. The detection limits were 50 ppm for Cl and 200 ppm for F in amphibole and mica.

Estimation of the bulk inclusion composition

Bulk chemical compositions of the MSI were obtained by two methods: (1) calculations using mineral modal compositions and microprobe analyses of the daughter phases; (2) direct microprobe analyses using an electron-beam raster-scan method covering the entire area of the MSI. Method (1) was employed for MSI in olivine (i.e. O-type and O'-type). The main difficulty of this method was in obtaining accurate modal analyses of single MSI because of their small size, limited exposures on the polished surface, limited numbers of MSI within a single thin section, and the presence of altered phases in some MSI. Moreover, some minerals showed compositional zoning, and thus errors arise depending on the choice of microprobe analysis for the calculations. The modal composition of the MSI was obtained for single inclusions by measuring the area of the daughter minerals traced on backscattered electron images with the aid of computer software. Inclusions whose minerals were heavily altered were avoided to minimize uncertainties in the modal analyses.

Three to seven MSI were chosen for each thin section and measured, and the average values were used for calculations with the assumption that all the inclusions had the same modal composition within the same thin section (Table A1 in the Appendix). The modal composition was converted to weight per cent using mineral density data given in the Mineralogy Database (2001, http://webmineral.com/). Special care was taken to avoid possible errors during the selection of representative mineral compositions, which are listed in Table A2 in the Appendix. Talc and hematite were counted as orthopyroxene because they are thought to be replacements after orthopyroxene.

Method (2) was mainly applied to P-type MSI because accurate modal analysis is more difficult for this type than the O- and O'-types. As described below, the P-type MSI are more fine-grained and it is difficult to identify and analyze all the phases included. A field emission scanning electron microscope (FE-SEM, JEOL JSM-6700F) equipped with an Oxford INCA Energy 350 system at Kyushu University was used for this purpose. Outlines of the P-type MSI were traced freehand and then X-ray counts were taken in raster-scan mode covering the entire area for each MSI. Because P-type MSI show more irregular shapes than the O- and O'-types and because the boundaries are blurred between the MSI and the host plagioclase, errors may arise while determining the exact boundaries for the P-type MSI. ZAF correction was employed, although this method requires re-correction of the results for systematic errors arising from the erroneous assumption of the samples being homogeneous. To test the consistencies of the results, the two methods were employed to obtain the bulk composition for one P-type MSI, whose mode was obtained with reasonable accuracy, and the results are compared in Table A3 in the Appendix. The result is satisfactory, justifying the comparison of the results obtained from the two methods.

MINERAL CHEMISTRY

Host olivine

Olivine is mostly homogeneous in terms of its Fe–Mg ratio except for the phenocrysts in the chilled marginal basalts. Figure 7 show a microprobe line traverse and Ca X-ray map of an olivine that hosts an O-type MSI in an olivine gabbro from the GR subzone. In contrast to the constant Fe/Mg ratio, the Ca content varies significantly and shows clear concentric zoning, although its content is low (0·1–0·3 wt %). The Ca content is highest (~0·3 wt %) in the olivine away from the MSI and decreases outwards and inwards (Fig. 7b and c).

Small olivine crystals included in resorbed plagioclase from the GR subzone (Fig. 6f) are higher in Fo content (~Fo_{70}) and lower in Ca content (<0·1 wt %) than the normal coarse-grained olivine ($Fo_{65–66}$, CaO = 0·1–0·3 wt %; i.e. primocrysts; Table 2, Fig. 2e).

Amphibole

Representative microprobe analyses of amphibole are given in Table 3 and their compositional variability is illustrated in Fig. 8 in relation to their mode of occurrence. Formula calculations including ferric–ferrous estimates were made on the basis of 13 cations following the method of Leake *et al.* (1997; 13eCNK) and Schumacher (1997). As mentioned in the petrography section, amphiboles in the O-type MSI are mostly pargasite (Fig. 8a and b), whereas those from the matrix (i.e. groundmass) outside the olivine and those from the O'-type MSI (i.e. chilled margins) are less pargasitic hornblende (Fig. 8b). Whereas most amphiboles in the O-type MSI contain hardly any F and Cl (below the detection limits), amphiboles from the matrix have significant F and Cl contents (F ~0·4 wt %, Cl ~0·14 wt %) (Table 3). More specifically, the brownish cores of the amphiboles in the O-type MSI (of the amphibole-dominant variety) are Ti-rich pargasite whereas their greenish rims are Ti-poor hornblende, which is comparable with the matrix amphiboles (Fig. 8a). Those from orthopyroxene-dominant varieties from the upper part of the AC subzone, however, do not have such a distinctly pargasitic core and the zoning is less pronounced (21 m and 36 m samples in Fig. 8b).

Figure 9 shows the details of a compositional zoning identified by microprobe analysis for an amphibole crystal from a typical O-type MSI (an amphibole-dominant variety from the GR subzone). The amphibole has a flat core of constant composition (pargasite); towards the rim the Mg content rapidly increases, whereas Al and Ca decrease complementarily, implying a rimward decrease in the Tschermak substitution. The decrease of Na content, on the other hand, only occurs near the margin of the grain, whereas the Ti content starts to decrease rimward much nearer the core. The total Fe content stays more or less constant until very near the margin, where it drops only slightly. Formula calculations show that the ferric–ferrous ratio increases towards the rim, where virtually all the iron becomes Fe^{3+}. Although absolute values depend on the methods and assumptions made in the formula calculations, the outward increase in the ferric–ferrous ratio is obtained no matter which method of calculation is employed and therefore is considered valid. This observed increase in the ferric–ferrous ratio is important because it may imply progressive oxidation during the crystallization of amphibole within the inclusion as discussed below. The observed increase in the Mg-number [i.e. $Mg/(Mg + Fe^{2+})$] in the zoning pattern (Fig. 9) is thus probably simply due to intra-inclusion progressive oxidation of iron. To test this hypothesis, we compared the variation and correlation of the Mg-numbers of amphiboles, estimated using two different assumptions, with those of other mafic phases, as

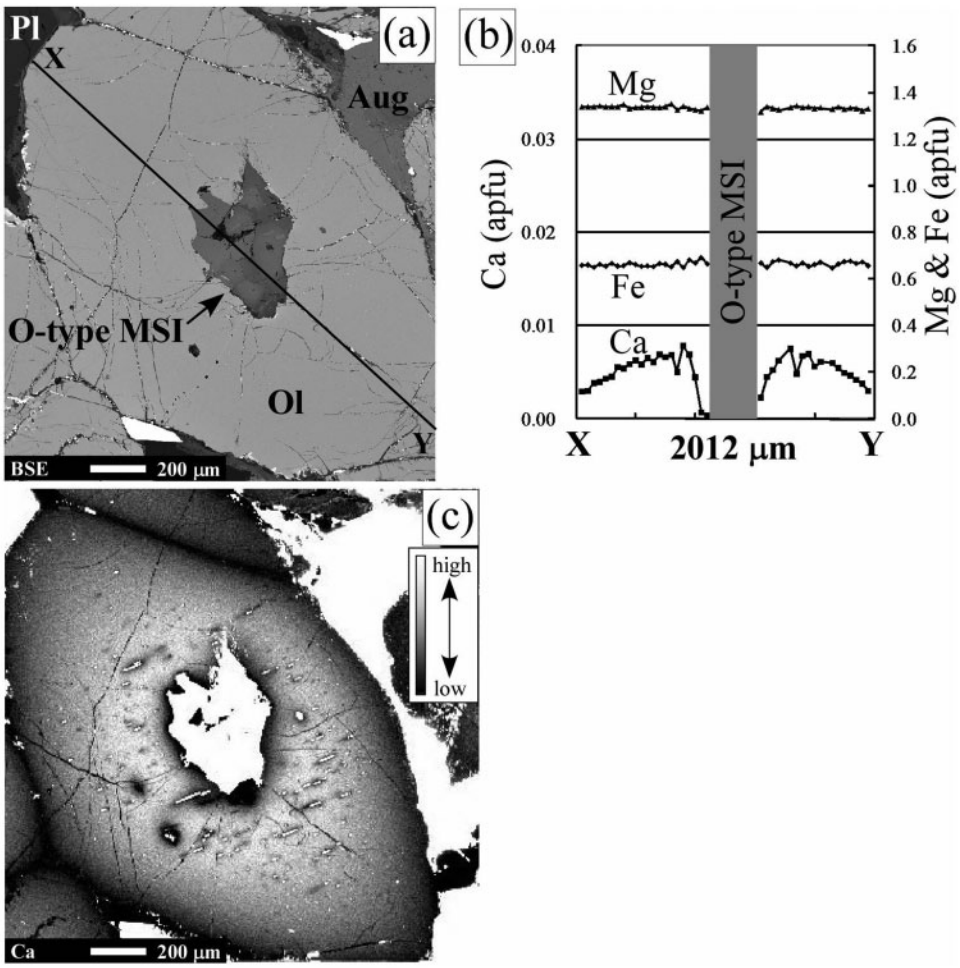

Fig. 7. (a, b) A line traverse of an olivine that includes an O-type MSI, taken along section X–Y in (a) (GR subzone, 71 m from the base; sample 92080706). (c) Ca X-ray map of the same olivine, obtained by WDS analysis.

shown in a stratigraphic variation diagram in Fig. 10. A better correlation was obtained if total Fe was assumed to be all Fe^{2+} rather than the calculated Fe^{2+}, for orthopyroxene, bulk MSI, and host olivines (Fig. 2e), which supports the hypothesis that the oxidation of Fe in amphibole is an intra-inclusion event during the fractional crystallization of amphibole and is unrelated to the orthopyroxene and olivine hosts.

Orthopyroxene

Representative microprobe analyses of orthopyroxene, both from the O- and O'-type MSI and from the matrices outside of the olivine hosts, are given in Table 4. Compositional variations of orthopyroxenes from the O-type MSI and the matrix are illustrated in SiO_2–CaO and SiO_2–Al_2O_3 plots in Fig. 11. The orthopyroxenes from the O-type MSI are more variable in Si, Al, and Ca content than those from the matrix and, on average, are higher in Al and Ca and lower in Si content than those from the matrix (Table 4, Fig. 11). The orthopyroxenes adjacent to the olivine wall in the O-type MSI (Table 4, see table legend) have a higher Mg-number (72–73) and a lower Al content than those from the inner side of the inclusions. The stratigraphic variation of the Mg-number of orthopyroxene (Fig. 10b) is positively correlated with that of the Fo content of olivine (Fig. 2e).

Clinopyroxene

Representative microprobe analyses of clinopyroxene from MSI and their matrix are given in Table 5, and their compositional variations are illustrated in Fig. 12. Similar to orthopyroxene, clinopyroxene in the O-type MSI is more Tschermakitic than that in the matrix. Conversely, Ti content is lower in the MSI clinopyroxene than in the matrix clinopyroxene.

Biotite and aspidolite

Representative microprobe analyses of the biotite-like phases are given in Table 6. Formula calculations were made assuming that all iron was ferrous. Some greenish

Table 2: Microprobe analyses of olivine

Ref. no.:	1	2	3	4	5	6	7	8	9	10
Zone:	Chilled margin	LZ (AC subzone)			LZ (GR subzone)					UZ
Sample:	92080907	92080901	92080912	91080507	ML	91080708	92080701	92080706	92080706	92081003
Height (m):	0	7	21	36	43	62	66	71	71	209
n:	2	11	4	3	22	16	16	15	7	8
SiO_2	40·4	38·5	36·7	36·7	36·5	37·0	37·4	37·8	38·3	37·9
FeO	16·7	23·4	30·5	32·4	34·3	30·3	29·9	29·8	27·2	29·8
MnO	0·19	0·35	0·46	0·49	0·58	0·51	0·51	0·49	0·52	0·56
MgO	44·0	38·7	32·1	31·5	29·2	32·6	32·5	32·5	34·7	32·5
CaO	0·21	0·09	0·09	0·09	0·28	0·23	0·21	0·19	0·08	0·07
NiO	0·27	0·16	n.a.	n.a.	0·08	0·08	0·08	0·09	0·08	0·13
Total	101·8	101·3	100·4	101·2	101·0	100·7	100·6	100·9	101·02	101·00
Cations per 4 oxygens										
Si	1·005	0·995	0·997	0·998	1·000	0·996	1·004	1·010	1·010	1·011
Fe	0·347	0·505	0·693	0·716	0·787	0·682	0·672	0·665	0·600	0·665
Mn	0·004	0·008	0·011	0·012	0·013	0·012	0·011	0·011	0·011	0·013
Mg	1·628	1·491	1·300	1·273	1·190	1·307	1·300	1·296	1·364	1·295
Ca	0·006	0·003	0·003	0·002	0·008	0·007	0·006	0·005	0·002	0·002
Ni	0·005	0·003	n.a.	n.a.	0·002	0·002	0·002	0·002	0·002	0·003
Total	2·995	3·005	3·003	3·002	3·000	3·004	2·996	2·990	2·990	2·989
Mg-no.	82·4	74·7	65·2	64·0	60·2	65·7	65·9	66·1	69·4	66·1

n, number of spot analyses to obtain the averages. No. 9 is average of small olivine crystals included in resorbed part of plagioclase. n.a., not analyzed. Other abbreviations are the same as in Fig. 2.

micas in the O-type MSI gave anomalously low totals (91–94 wt %) with lower total alkalis and lower Ti contents than the others, and therefore, they were considered to be alteration products.

Apart from the alteration, there originally appear to have been two kinds of mica in the O-type MSI: K-rich mica (biotite) and Na-rich mica (aspidolite). Biotite also occurs in the matrix, whereas aspidolite occurs only in the O-type MSI (Fig. 3h); in some cases, aspidolite forms composite grains with ordinary biotite (Fig. 3c). Aspidolite has been known to occur in MSI in chromite and Al-spinels from several other localities (e.g. Li *et al.*, 2005; Spandler *et al.*, 2005; Renna & Tribuzio, 2011).

BULK COMPOSITION OF THE MULTIPHASE SOLID INCLUSIONS

Apart from the errors in the modal mineralogy of the MSI as mentioned above, an important source of error in estimating the bulk compositions of the MSI by method (1) is the zoning and inhomogeneities of daughter phases, such as amphibole, orthopyroxene, and mica. For orthopyroxene, we used intermediate compositions between the rim and core compositions. For zoned amphiboles in O-type MSI, we used average compositions after evaluating the zoning of the amphibole (Fig. 9). For micas in O-type MSI, we used the aspidolite composition. The use of the biotite composition instead of the aspidolite composition for estimating the MSI bulk compositions results in an increase in K_2O content from 0·1 to 1·6 wt % and a decrease in Na_2O content from 2·7 to 1·3 wt %. The variation of the other major element contents for this choice of mica composition is restricted to within 3% at most and should not influence the discussion below. Because a microprobe analysis of aspidolite in the O-type MSI from the 62 m sample was not available, we used instead the 71 m sample data for the calculation. All of the values used in the calculations are listed in Table A2 in the Appendix.

The bulk compositions of the MSI averaged for each sample are listed in Table 7, which includes one analysis of O'-type (from the lower chilled margin), two O-types from the AC subzone, two O-types from the GR subzone [all of which were obtained by method (1)], and an average

Table 3: Representative microprobe analyses of amphibole

Ref. no.:	1	2	3	4	5	6	7	8	9	10	11	12	13	14	15	16	17	18	19
Zone:	chilled margin	AC							GR										
Sample:	LCM32		92080901		92080912			91080507		ML1	ML3	91090708							92080706
Height (m):	0		7		21			36		43		62							71
Type:	O′-type	O′-type	O-type	Matrix	O-type	O-type	Matrix	O-type	O-type	O-type	O-type	O-type	O-type	O-type	P-type	P-type	Matrix	Matrix	O-type
Position:			core							core	core	core	rim	rim	core	rim			
SiO_2	46·4	49·0	40·7	46·3	45·2	41·9	44·1	44·8	43·9	40·4	38·8	41·6	46·5	52·5	44·7	43·5	45·7	46·5	42·4
TiO_2	1·73	1·72	4·81	3·49	1·22	1·62	3·60	2·73	2·27	3·49	4·50	3·92	0·25	0·17	2·95	2·54	2·75	2·83	1·47
Al_2O_3	10·7	9·11	12·8	7·28	10·6	12·4	9·09	9·18	9·70	13·9	14·4	12·4	9·15	3·23	9·51	9·86	7·83	7·32	12·2
Cr_2O_3	n.a.	n.a.	0·08	0·08	0·20	0·08	0·02	0·01	0·02	0·05	0·02	n.a.	n.a.	n.a.	n.a.	n.a.	n.a.	n.a.	n.a.
FeO	6·93	5·47	10·5	8·74	11·4	13·0	12·8	13·3	12·1	13·6	12·5	12·4	12·6	9·67	12·3	15·9	12·0	11·8	12·3
MnO	0·12	0·27	0·17	0·18	0·14	0·12	0·19	0·21	0·18	0·18	0·20	0·15	0·19	0·22	0·32	0·28	0·20	0·19	0·14
MgO	17·2	18·6	13·2	16·2	15·0	13·8	13·8	14·7	14·5	11·4	11·2	13·1	17·2	20·3	14·7	11·4	15·9	15·6	14·3
CaO	11·4	11·5	10·7	9·51	10·3	9·38	10·3	7·71	8·88	11·0	11·0	11·3	9·16	9·39	10·4	11·8	10·3	10·0	10·9
Na_2O	2·37	1·95	3·75	3·23	3·59	3·72	2·76	4·47	4·53	3·58	3·88	3·55	2·89	1·18	3·06	2·83	2·64	3·16	3·57
K_2O	0·32	0·23	0·03	0·32	0·07	0·11	0·38	0·15	0·03	0·04	0·07	0·03	0·12	0·05	0·26	0·47	0·44	0·42	0·16
F	0·00	0·00	0·00	0·40	0·02	0·00	0·22	0·00	0·00	n.a.	n.a.	n.a.	n.a.	n.a.	n.a.	n.a.	n.a.	n.a.	0·07
Cl	0·00	0·00	0·01	0·02	0·01	0·02	0·09	0·05	0·01	n.a.	n.a.	n.a.	n.a.	n.a.	n.a.	n.a.	n.a.	n.a.	n.a.
H_2O*	2·12	2·16	2·03	1·86	2·08	2·06	1·92	2·08	2·05	2·03	1·99	2·06	2·14	2·15	2·09	2·02	2·10	2·09	2·04
O = F, Cl	0·00	0·00	0·00	0·17	0·01	0·00	0·11	0·01	0·00	0·00	0·00	0·00	0·00	0·00	0·00	0·00	0·00	0·00	0·03
Total	99·8	100·6	99·0	98·0	100·6	99·4	99·7	100·6	99·1	99·9	98·6	100·8	101·6	100·0	101·1	100·8	100·9	100·5	100·4
Formula based on 23 oxygen atoms and assuming a total of 13 cations exclusive of Ca, Na and K																			
Si	6·56	6·81	6·00	6·75	6·48	6·09	6·45	6·42	6·41	5·98	5·83	6·06	6·53	7·33	6·41	6·45	6·54	6·68	6·14
Ti	0·18	0·18	0·53	0·38	0·13	0·18	0·40	0·29	0·25	0·39	0·51	0·43	0·03	0·02	0·32	0·28	0·30	0·31	0·16
Al	1·79	1·49	2·23	1·25	1·79	2·12	1·57	1·55	1·67	2·42	2·55	2·13	1·51	0·53	1·61	1·72	1·32	1·24	2·09
Fe^{3+}†	0·54	0·55	0·21	0·53	0·80	1·34	0·67	1·40	0·94	0·32	0·07	0·36	1·48	1·13	0·82	0·14	1·03	0·76	0·89
Fe^{2+}†	0·28	0·09	1·08	0·54	0·56	0·25	0·89	0·19	0·54	1·36	1·50	1·15	0·00	0·00	0·65	1·84	0·40	0·66	0·60
Mn	0·01	0·03	0·02	0·02	0·02	0·02	0·02	0·02	0·02	0·02	0·03	0·02	0·02	0·03	0·04	0·04	0·02	0·02	0·02
Mg	3·63	3·85	2·91	3·52	3·20	3·00	3·00	3·13	3·17	2·50	2·52	2·85	3·60	4·23	3·15	2·53	3·39	3·33	3·10
Ca	1·73	1·71	1·70	1·48	1·58	1·46	1·61	1·18	1·39	1·74	1·78	1·76	1·38	1·40	1·61	1·88	1·58	1·53	1·69
Na	0·65	0·53	1·07	0·91	1·00	1·05	0·78	1·24	1·28	1·03	1·13	1·00	0·79	0·32	0·85	0·82	0·73	0·88	1·00
K	0·06	0·04	0·01	0·06	0·01	0·02	0·07	0·03	0·01	0·01	0·01	0·00	0·02	0·01	0·05	0·09	0·08	0·08	0·03
F	0·00	0·00	0·00	0·18	0·01	0·00	0·10	0·00	0·00	0·00	0·00	0·00	0·00	0·00	0·00	0·00	0·00	0·00	0·03
Cl	0·00	0·00	0·00	0·00	0·00	0·00	0·02	0·01	0·00	0·00	0·00	0·00	0·00	0·00	0·00	0·00	0·00	0·00	0·00
OH	2·00	2·00	2·00	1·81	1·99	2·00	1·88	1·99	2·00	2·00	2·00	2·00	2·00	2·00	2·00	2·00	2·00	2·00	1·97
Total	17·4	17·3	17·8	17·5	17·6	17·5	17·5	17·4	17·7	17·8	17·9	17·8	17·4	17·0	17·5	17·8	17·4	17·5	17·7
mg-no.‡	92·9	97·7	72·9	86·8	84·8	80·0	77·1	94·3	85·4	64·8	62·7	71·1	100·0	100·0	82·8	57·9	89·3	83·5	83·7

*H_2O calculated assuming stoichiometry.
†Fe^{3+} and Fe^{2+} calculated assuming 23 O per formula unit and cation total of 13 excluding Ca, Na and K.
‡mg-no. $= Mg/(Mg + Fe^{2+}) \times 100$.
Matrix, amphibole outside olivine crystals. n.a., not analyzed. Other abbreviations are the same as in Fig. 2.

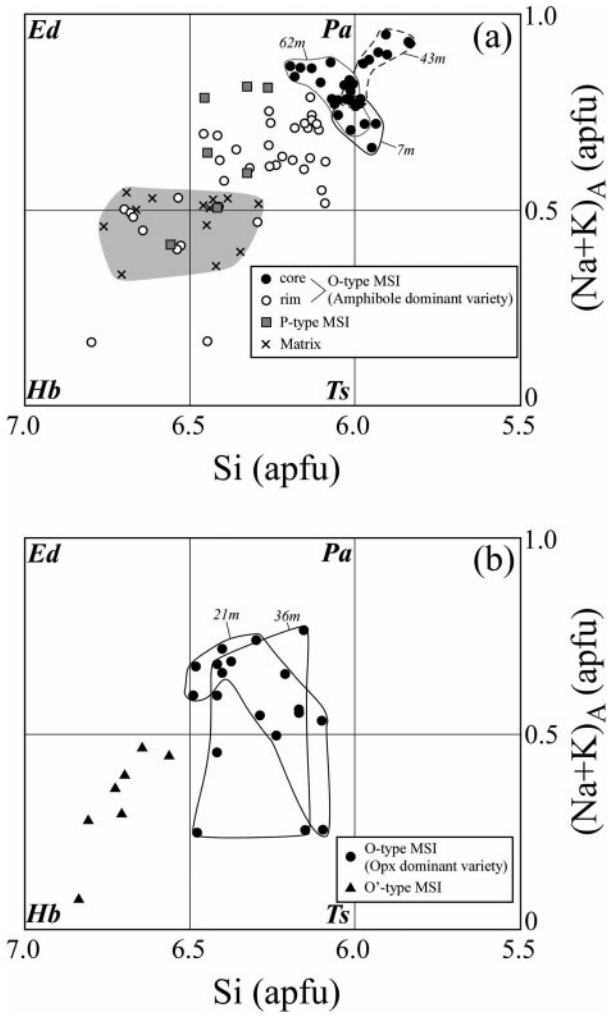

Fig. 8. Compositional variation of amphiboles from three types of MSI and those from the matrix. (a) Amphiboles from amphibole-dominant O-type and P-type MSI. Core compositions are indicated for each sample by continuous and dashed gray lines. Numbers are the stratigraphic position of each sample (in m). Shaded area indicates the compositional field of the matrix amphibole. (b) Amphiboles from orthopyroxene-dominant O-type MSI and from the O'-type MSI. Data from the O-type MSI are highlighted for each sample with continuous lines (numbers are the positions of the samples). Core–rim distinction is not made in (b) because zoning is not as distinct as in (a).

composition of P-type MSI [obtained by method (2)] from two samples from the GR subzone. Statistically obtained 1σ values are reported for each average to show the analytical dispersion. The inferred initial melt composition of the intrusion (Akatsuka *et al.*, 1999) is also given for comparison. The data are plotted in variation diagrams in Fig. 13 and are compared with the whole-rock compositions of the intrusion (Akatsuka *et al.*, 1999) and with the inferred fractionation trend of the Murotomisaki Gabbro initial melt, which was derived using the PELE software (Boudreau, 1999*a*). Calculations were made starting from the initial melt composition of the intrusion (Akatsuka *et al.*, 1999), assuming 1 wt % H_2O in of the initial melt—a typical value for fresh tholeiitic basalts (McBirney, 1993). We also assumed NNO (nickel–nickel oxide) for the oxygen buffer and 1 kbar for the pressure of crystallization (Yajima *et al.*, 1977).

The bulk compositions of the O'-type MSI are closest to the initial melt composition IM, but have higher SiO_2 and MgO and lower FeO contents than IM (Table 7). A notable characteristic is the high Mg-number, which is comparable with that of the host olivine (Fig. 10a). The O-type MSI have even higher MgO contents. The FeO contents are comparable with and the Al_2O_3 contents are considerably less than those of IM. They also have a high Mg-number, which is again comparable with that of their host olivines. The P-type MSI, on the other hand, have different compositions from the O'- and O-type MSI, even considering their larger uncertainties. The SiO_2 content is comparable, but their Al_2O_3 and CaO contents are fairly high, and the FeO and MgO amounts are considerably less than those of IM. Their Mg-number is closest to that of IM. The compositional scatter of the P-type MSI may be accounted for primarily in terms of the variable proportion of plagioclase and amphibole with a subordinate amount of Ti-magnetite and apatite. In other words, the P-type MSI appear to be enriched in plagioclase components with respect to IM. However, the O-type MSI are anomalous, being enriched in olivine components. Some MSI compositions plot close to the bulk compositions of some olivine gabbros in the AC zone (Fig. 13). The O'-type MSI plot closest to IM, but their FeO contents are low and have considerably higher Mg-numbers as mentioned above. More detailed consideration is given in the discussion below.

DISCUSSION

Origin of O'-type MSI

It became apparent from examining the bulk compositions of MSI from the Murotomisaki Gabbro that many of these MSI do not simply represent trapped melts. More complex processes may have to be considered to account for their compositions. Among the three types of MSI, the O'-type MSI (i.e. in the chilled margins) appears to be the most tractable in terms of their origin. Judging from the textures and bulk compositions, it is most likely that the O'-type MSI are closest to the melt entrapped in growing phenocrysts of olivine. Because the growth of olivine phenocrysts must generally occur at great depths and not during quenching after emplacement, the melt entrapment must have occurred well before the final emplacement of the magmas. Melt entrapment in phenocrystic olivines is known to occur commonly in volcanic rocks

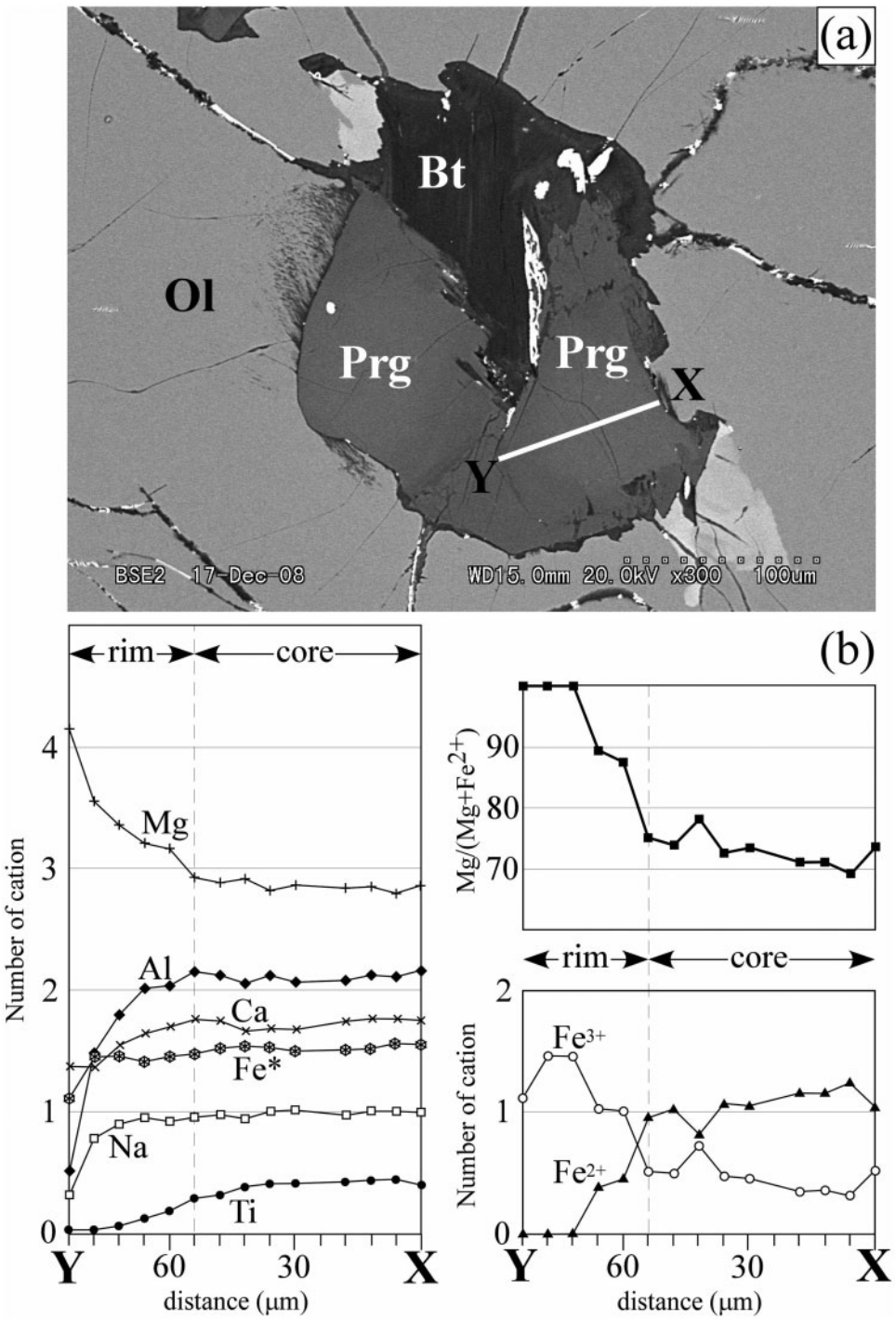

Fig. 9. A compositional line profile for a single grain of amphibole in an O-type MSI. (a) Back-scattered electron (BSE) image of an O-type MSI from a GR subzone olivine gabbro, 91080708 (62 m from the base). (b) The line profile of the amphibole, taken along section X–Y in (a). Fe* is total iron; Fe^{2+} estimated from formula calculations (see text).

(e.g. Metrich & Clocchiatti, 1989; Gaetani & Watson, 2000).

When it comes to the bulk compositions, however, a problem remains: as noted above, the O'-type MSI composition is much lower in FeO and higher in MgO than the published initial melt composition (IM) of the intrusion (Akatsuka *et al.*, 1999). Considering that its Mg-number is comparable with that of the present host

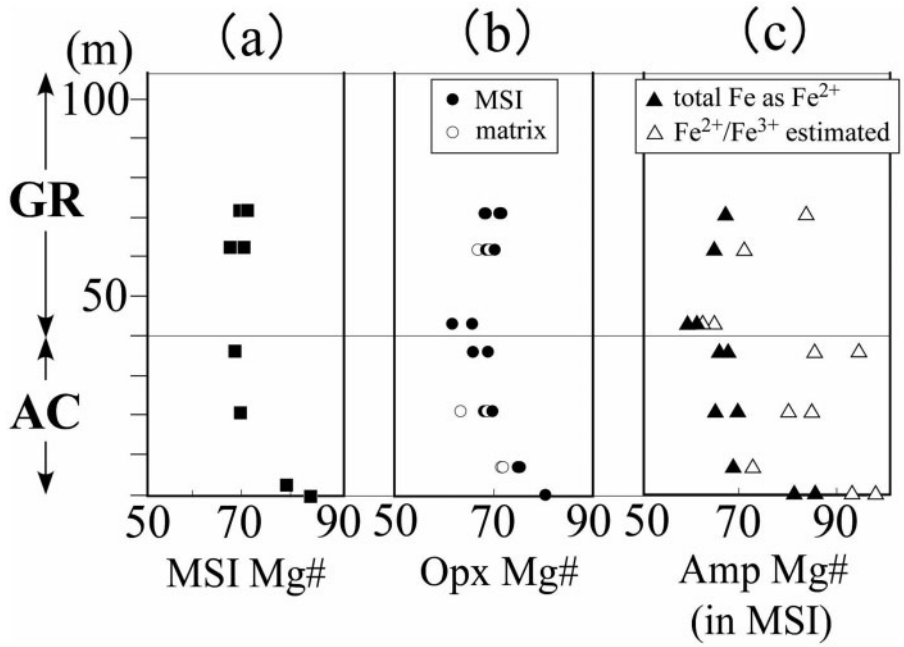

Fig. 10. Mg-numbers [Mg/(Mg + Fe) × 100] of bulk MSI of O-type and O'-type (a), of orthopyroxenes from the MSI and the matrices (b), and of amphiboles (core only) from the MSI (c). For amphiboles only, another Mg-number [$Mg/(Mg+Fe^{2+}) \times 100$] using Fe^{2+} estimated from the formula calculation is also plotted for comparison (open triangles).

olivine (Fo_{83}), it is likely that the O'-type MSI attained Fe–Mg exchange equilibrium with their host olivines, thereby experiencing a decrease of Fe and an increase of Mg during or after solidification of the trapped melt. This process has been discussed and was referred to as 'Fe-loss' by Danyushevsky *et al.* (2000). To test this hypothesis we made a correction calculation to retrieve the original melt composition by applying an Fe–Mg exchange to the observed MSI composition (the increase and the decrease of equimolar amounts of FeO and MgO, respectively) in a similar manner to Danyushevsky *et al.* (2000). We applied the correction so that the hypothetical original melt achieves Fe–Mg exchange equilibrium with the host olivine (Fo_{83}), assuming $K_D(Fe–Mg)^{ol–liq} = 0{\cdot}30 \pm 0{\cdot}03$ (Roeder & Emslie, 1970). The result of the calculation is given in Table 8 and shown in Fig. 14. The corrected compositions (i.e. hypothetical melt compositions) are now closer to the initial melt composition (IM) of Akatsuka *et al.* (1999) (Fig. 14), which supports our inference that the O'-type MSI represent trapped and then Fe–Mg ratio-modified melts in growing crystals of olivine.

Origin of O-type MSI

From their textural appearance, it is likely that the O-type MSI also represent trapped melts, but their bulk compositions are different from those of the O'-type MSI, as noted above. Considering the much slower cooling rate in the AC and GR subzones than in the chilled margin, modification of the MSI bulk composition via diffusion as considered for the O'-type is expected to have been more thorough than in the chilled margin. We therefore applied the same correction to the bulk compositions of the O-type MSI as we did to the O'-type MSI. The results are shown in Table 8 and in Fig. 14. It is noted that host olivines from the AC and GR subzones are rather homogeneous with respect to Mg-number and are more Fe-rich than the phenocrystic olivines in the chilled margin. From this fact, a possibility arises that olivine re-equilibrated with the ambient fractionated interstitial melt and homogenized to become more Fe-rich since the entrapment of the melt. That is, the olivine at the time of melt entrapment may have been more Mg-rich than it is at present. Without knowing the exact olivine compositions at the time of melt entrapment, we made calculations assuming two olivine compositions as extreme cases: (a) Fo_{83}, the most magnesian, chilled marginal value; (b) Fo_{65}, an average present host olivine value in the GR subzone. The Mg-numbers for the hypothetical melts that are supposed to be in equilibrium with these olivines are 60 and 35, respectively, assuming $K_D = 0{\cdot}30$. The results are tabulated in Table 8 and illustrated in Fig. 14. Although we cannot accurately estimate the trapped melt composition because of the uncertainty of the composition of the equilibrium olivine, we can safely conclude that the true values were somewhere between these two extremes [i.e. (a) and (b) in Table 8 and Fig. 14]. Neither (a) nor (b) matches IM

Table 4: Representative microprobe analyses of orthopyroxene

Ref. no.:	1	2	3	4	5	6	7	8	9	10	11	12	13	14	15	16	17	18	19	20	21
Zone:	chilled margin	AC										GR									
Sample:	LCM32	92080901				92080912				91080507		ML1		91090708				92080706			
Height (m):	0	7				21				36		43		62				71			
Type:	O′-type	O-type	O-type	Matrix	Matrix	O-type	O-type	Matrix	Matrix	O-type	O-type	O-type	O-type	O-type	O-type	Matrix	Matrix	O-type	O-type*	O-type	O-type*
SiO_2	55·0	54·5	53·2	53·9	53·7	52·4	54·6	53·9	52·9	53·6	53·0	52·6	53·0	54·8	51·2	54·0	53·9	52·7	55·8	52·3	55·3
TiO_2	0·38	0·15	0·13	0·00	0·08	0·18	0·02	0·24	0·00	0·00	0·20	0·05	0·05	0·02	0·31	0·22	0·23	0·49	0·03	0·06	0·00
Al_2O_3	2·89	1·25	4·05	1·78	1·19	2·33	0·45	0·54	1·38	0·41	1·77	2·73	1·89	0·12	3·39	0·34	0·34	3·41	0·67	4·27	0·76
FeO	11·5	15·7	15·0	17·6	17·5	19·1	18·8	19·1	22·2	21·1	19·2	20·6	22·8	18·8	18·7	19·1	20·9	18·7	17·6	18·9	17·7
MnO	0·27	0·38	0·37	0·44	0·43	0·54	0·49	0·41	0·51	0·54	0·44	0·52	0·62	0·50	0·45	0·47	0·43	0·53	0·44	0·48	0·44
MgO	27·9	27·9	26·2	26·0	26·1	23·7	25·4	24·7	22·4	23·4	24·8	23·0	21·3	25·8	23·6	24·8	24·6	23·5	26·0	23·7	25·6
CaO	2·30	1·06	1·08	0·26	0·44	1·18	0·37	1·07	0·58	0·37	0·39	1·25	1·22	0·31	1·41	1·16	1·06	1·71	0·67	1·37	0·84
Na_2O	0·43	0·05	0·04	0·03	0·04	0·00	0·05	0·03	0·00	0·07	0·02	0·03	0·05	0·05	0·02	0·04	0·04	0·04	0·00	0·08	0·03
Total	100·6	101·0	100·1	100·1	99·4	99·3	100·1	100·1	100·0	99·5	99·8	100·8	101·0	100·4	99·1	100·2	101·4	101·1	101·3	101·1	100·7
Formula based on 3 oxygen atoms																					
Si	0·97	0·98	0·96	0·98	0·98	0·97	1·00	0·99	0·98	1·00	0·97	0·97	0·98	1·00	0·95	0·99	0·98	0·96	1·00	0·95	1·00
Ti	0·01	0·00	0·00	0·00	0·00	0·00	0·00	0·00	0·00	0·00	0·00	0·00	0·00	0·00	0·00	0·00	0·00	0·01	0·00	0·00	0·00
Al	0·06	0·03	0·09	0·04	0·03	0·05	0·01	0·01	0·03	0·01	0·04	0·06	0·04	0·00	0·07	0·01	0·01	0·07	0·01	0·09	0·02
Fe	0·17	0·24	0·22	0·27	0·27	0·29	0·29	0·29	0·35	0·33	0·29	0·32	0·35	0·29	0·29	0·29	0·32	0·28	0·26	0·29	0·27
Mn	0·00	0·01	0·01	0·01	0·01	0·01	0·01	0·01	0·01	0·01	0·01	0·01	0·01	0·01	0·01	0·01	0·01	0·01	0·01	0·01	0·01
Mg	0·73	0·74	0·70	0·70	0·71	0·65	0·69	0·68	0·62	0·65	0·68	0·63	0·59	0·70	0·65	0·68	0·67	0·64	0·69	0·64	0·69
Ca	0·04	0·02	0·02	0·00	0·01	0·02	0·01	0·02	0·01	0·01	0·01	0·02	0·02	0·01	0·03	0·02	0·02	0·03	0·01	0·03	0·02
Na	0·01	0·00	0·00	0·00	0·00	0·00	0·00	0·00	0·00	0·00	0·00	0·00	0·00	0·00	0·00	0·00	0·00	0·00	0·00	0·00	0·00
Total	2·00	2·01	2·00	2·00	2·00	2·00	2·00	2·00	2·00	2·00	2·00	2·00	2·00	2·00	2·01	2·00	2·01	2·00	1·99	2·01	1·99
Mg-no.	81·2	75·9	75·7	72·5	72·6	68·9	70·6	69·8	64·2	66·5	69·7	66·6	62·4	71·0	69·3	69·9	67·7	69·2	72·5	69·1	72·1

*Opx in the O-type MSI, adjacent to the olivine wall (distance from the wall is less than 30 μm). Other orthopyroxenes from the 71 m sample are more than 30 μm away from the wall.
Other abbreviations are the same as in Fig. 2.

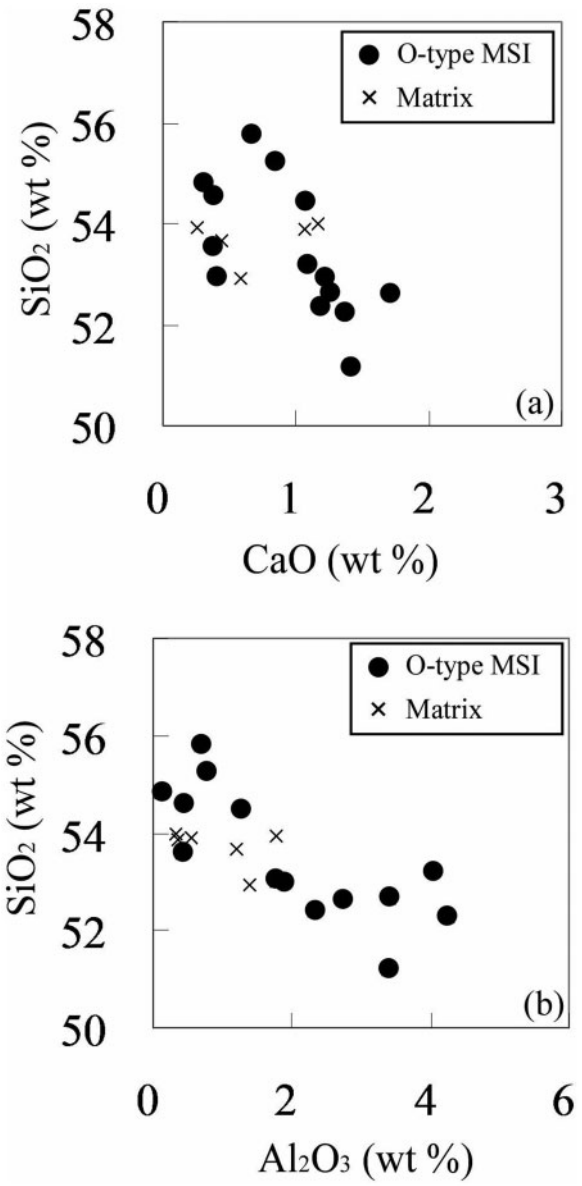

Fig. 11. Compositional variations of orthopyroxenes from the O-type MSI and the matrix. (a) SiO_2–CaO and (b) SiO_2–Al_2O_3 (wt %) plots. Sample 91080912 (21 m from the base).

(Table 8) and it is obvious from Fig. 14 that the hypothetical melts (deduced from the O-type MSI) are remote, in composition, from IM or any fractionated derivatives of it and that they lie between the IM and the olivine compositions.

We considered so far a modification of the bulk composition by means of Fe–Mg diffusional exchange only, but we may also have to consider the effect of diffusional modification for other elements. For example, the lower Al_2O_3 and CaO contents of the O-type MSI compared with typical basaltic compositions may be ascribed to a loss of these components towards the ambient melts by diffusion through the host olivine. To assess this possibility, we examined the mobilities of these elements by diffusion in olivine using available experimental data. The average diffusion coefficient of Ca in olivine during linear cooling from liquidus temperatures to about 900°C at the GR subzone (70 m horizon) may be obtained using the Arrhenius equation from the experiments by Coogan *et al.* (2005) as $1{\cdot}4\times10^{-17}$ to $3{\cdot}4\times10^{-18}$ (m^2 s^{-1}) ($fO_2=10^{-8}$–10^{-10}). Using these values, the diffusion distance during this cooling is estimated to be about 150–300 μm. In fact, because cooling may have been faster because of thermal and compositional convection, the estimated diffusion distance should be regarded as an upper bound. Therefore, Ca in an O-type MSI cannot reach within the estimated time the outside of the host olivine (1000–2000 μm size, Fig. 7). The Ca loss by diffusion, even if it had occurred, would have been at most as much as the present host olivine (about 0·3 wt %, Table 2). Although there is no direct experimental measurement, the diffusivity of Al in olivine is likely to be much less than that of Fe and Mg (Scowen *et al.*, 1991; Milman-Barris *et al.*, 2008). Therefore, the low Ca and Al character of the O-type MSI cannot be attributed to diffusive loss.

From this analysis, we conclude that the anomalous nature of the O-type MSI melt (i.e. rich in Fe and Mg, and poor in Ca and Al) cannot be derived from the ordinary melts derived by crystallization differentiation of the MGI basaltic melt but instead represent a primary feature of the trapped melts. Next, we consider the origin of such anomalous melts that formed the O-type MSI.

Origin of the O-type MSI melts

The liquid immiscibility hypothesis

Jakobsen *et al.* (2005) found that Fe-rich and Si-rich immiscible liquids were contained as crystallized melt inclusions (MSI in our notation) in primocrysts (olivine and apatite) from the Layered Series of the Skaergaard intrusion. According to them, the Fe-rich liquids occur only in apatite, and the Si-rich liquids occur in both apatite and olivine. Jakobsen *et al.* (2011) also found that crystallized melt inclusions in plagioclase primocrysts are highly variable in composition, and they ascribed the variability to different proportions of mixtures of the Fe-rich and Si-rich immiscible liquids.

The Fe–Mg corrected melt compositions of the O-type MSI are very Fe-rich particularly when the present olivine composition is assumed to be an equilibrium counterpart [melt (b) in Table 8, Fig. 14]. In fact, some of these compositions show some resemblance to the Fe-rich counterparts of immiscible silicate liquids that have been found in

Table 5: Representative microprobe analyses of clinopyroxene

Ref. no.:	1	2	3	4	5	6	7	8	9	10	11	12	13	14
Zone:	AC		GR											
Sample:	92080901		91080708-1				92080706							
Height (m):	7		62				71							
Type:	O-type	Matrix	O-type	Matrix	Matrix	Matrix	O-type	O-type	O-type	Matrix	Matrix	Matrix	Matrix	Matrix
SiO_2	50·2	51·9	49·4	51·8	51·7	52·2	51·7	51·7	52·0	52·0	52·5	52·5	52·2	52·1
TiO_2	0·35	0·89	0·82	1·17	1·20	1·13	0·54	0·48	0·24	1·62	0·96	0·87	1·05	1·11
Al_2O_3	5·95	3·13	5·08	2·07	2·24	2·18	4·21	4·14	3·69	2·32	2·28	2·30	2·28	2·34
Cr_2O_3	0·09	0·80	0·03	0·02	0·00	0·00	0·00	0·01	0·01	0·00	0·03	0·04	0·00	0·00
FeO	7·79	6·90	10·1	9·65	9·17	9·79	9·23	9·69	8·92	8·97	8·89	8·57	9·42	9·16
MnO	0·21	0·20	0·24	0·22	0·18	0·31	0·21	0·28	0·25	0·25	0·30	0·24	0·28	0·22
MgO	14·0	15·8	13·1	14·8	14·5	14·9	13·9	13·9	14·3	14·7	14·8	15·1	14·9	14·7
CaO	21·4	20·7	20·4	19·8	20·4	19·7	20·2	20·0	20·8	20·1	19·9	19·9	19·6	19·8
Na_2O	0·47	0·45	0·47	0·40	0·45	0·46	0·36	0·43	0·47	0·46	0·44	0·47	0·44	0·46
NiO	0·12	0·00	0·00	0·04	0·02	0·00	n.a.	n.a.	n.a.	n.a.	n.a.	n.a.	n.a.	n.a.
Total	100·5	100·7	99·7	100·0	99·9	100·7	100·4	100·6	100·7	100·4	100·1	99·9	100·1	99·9
Formula based on 3 oxygen atoms														
Si	0·93	0·95	0·93	0·97	0·96	0·97	0·96	0·96	0·96	0·96	0·97	0·97	0·97	0·97
Ti	0·00	0·01	0·01	0·02	0·02	0·02	0·01	0·01	0·00	0·02	0·01	0·01	0·01	0·02
Al	0·13	0·07	0·11	0·05	0·05	0·05	0·09	0·09	0·08	0·05	0·05	0·05	0·05	0·05
Cr	0·00	0·01	0·00	0·00	0·00	0·00	0·00	0·00	0·00	0·00	0·00	0·00	0·00	0·00
Fe	0·12	0·11	0·16	0·15	0·14	0·15	0·14	0·15	0·14	0·14	0·14	0·13	0·15	0·14
Mn	0·00	0·00	0·00	0·00	0·00	0·00	0·00	0·00	0·00	0·00	0·00	0·00	0·00	0·00
Mg	0·38	0·43	0·37	0·41	0·40	0·41	0·38	0·38	0·39	0·41	0·41	0·42	0·41	0·41
Ca	0·42	0·41	0·41	0·40	0·41	0·39	0·40	0·40	0·41	0·40	0·40	0·39	0·39	0·39
Na	0·02	0·02	0·02	0·01	0·02	0·02	0·01	0·02	0·02	0·02	0·02	0·02	0·02	0·02
Ni	0·00	0·00	0·00	0·00	0·00	0·00	n.a.	n.a.	n.a.	n.a.	n.a.	n.a.	n.a.	n.a.
Total	2·01	2·01	2·01	2·00	2·00	2·00	2·00	2·00	2·01	2·00	2·00	2·00	2·00	2·00
Mg-no.	76·2	80·4	69·8	73·2	73·9	73·1	72·8	71·9	74·1	74·5	74·8	75·9	73·8	74·1

Abbreviations are the same as in Fig. 2.

experimental and natural examples (McBirney & Nakamura, 1974; Dixon & Rutherford, 1979; Philpotts, 1982), except for their high MgO contents. More troublesome is the lack of any clear evidence for the presence of silica-rich counterparts of the immiscible liquids anywhere in the MGI. P-type MSI are rather poor in SiO_2 and do not show any resemblance to the Si-rich immiscible liquids reported in the literature. The kind of host phases also does not match with the case of the Skaergaard intrusion as described by Jakobsen *et al.* (2005). For these reasons, we do not consider that the liquid immiscibility hypothesis can account for the origin of MSI of the Murotomisaki samples.

Generation of picritic melts by dissolution of olivine by fluid fluxing

We now consider another mechanism whereby melts are locally enriched in olivine and plagioclase components by their dissolution. Theoretically, dissolution of silicates may be induced by an introduction of H_2O into crystal–melt systems (e.g, McBirney, 1987; Boudreau, 1999*b*). Hoshide & Obata (2009) discussed the possibility of hydrous flux melting of silicates in the GR subzone of the MGI. They concluded that significant dissolution of plagioclase took place in the MGI magma via the depression of the plagioclase liquidus caused by the introduction of H_2O-rich fluids derived from a fluid-saturated zone

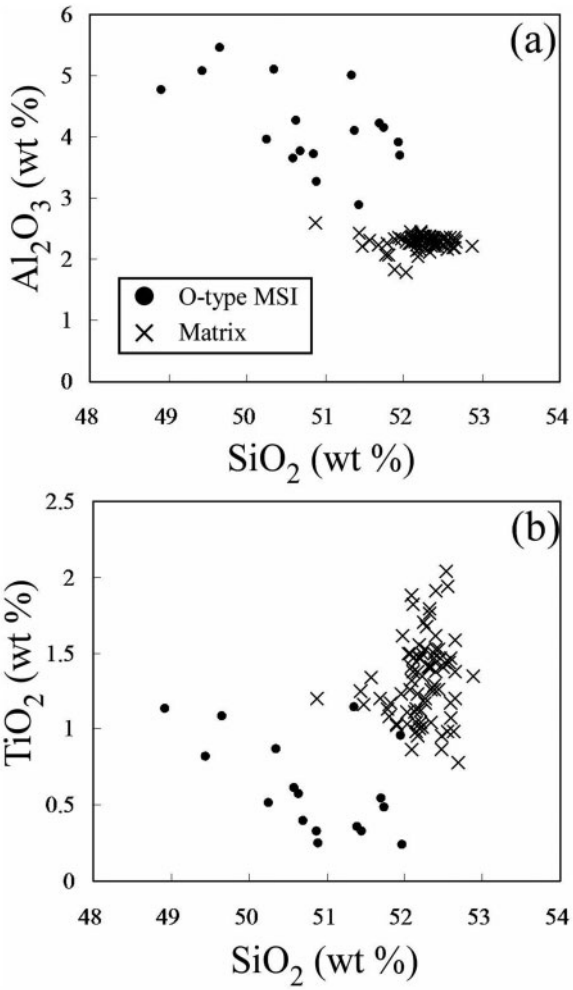

Fig. 12. Compositional variations of clinopyroxenes from the O-type MSI and the matrix. (a) SiO_2–Al_2O_3 and (b) SiO_2–TiO_2 plots.

lying below (Hoshide & Obata, 2009, fig. 11). They considered that H_2O-rich bubbles rose by buoyancy from the low-temperature, fluid-saturated zone to a higher-temperature and fluid-undersaturated horizon within a lower, partially crystallizing boundary layer of a magma system. Rising H_2O bubbles would dissolve again in the melt as they entered the H_2O-undersaturated zone, thereby raising the activity (or concentration) of H_2O there. As the H_2O fluid dissolved in the H_2O-undersaturated melt, P_{H_2O} in the melt would increase. Because the increase of P_{H_2O} in the basaltic melts would depress the plagioclase liquidus and the olivine liquidus (Medard & Grove, 2008), the H_2O-added melt should become undersaturated with both plagioclase and olivine. Then, plagioclase and olivine crystals would stop growing and start to dissolve into the melt. The dissolution was probably very local, creating inhomogeneities in the melt on a scale of the grain size, because of the limited diffusivities of elements in the melt (Hofmann, 1980; Chen & Zhang, 2008) and limited time for homogenization by diffusion; thereby H_2O-rich picritic melts would occur only around the dissolving olivine, and, likewise, plagioclase-rich melts would occur around the dissolving plagioclase. Because this part of the magma body continues cooling, olivine and plagioclase, which were once partly dissolved, eventually start to grow again. This is the time when the anomalous melts that were generated around the dissolved crystals were entrapped by these secondarily growing crystals. Whether or not the anomalous melts are entrapped by the growing crystals before they become homogenized by diffusion depends on the cooling and crystallization rate and requires more quantitative evaluation with more experimental data on diffusion and crystallization kinetics.

Origin of P-type MSI

P-type MSI may not have been affected by Fe–Mg exchange modification because the host phase, plagioclase, is virtually Fe- and Mg-free. Jakobsen *et al.* (2011) pointed out the possibility of significant loss of alkalis into the plagioclase host. They suggested that albitic plagioclase rims around plagioclase-hosted melt inclusions in the Skaergaard intrusion were formed by loss of alkalis. However, in the Murotomisaki samples, anorthitic plagioclase (i.e. high-An edge) rather than albitic plagioclase occurs around the P-type MSI. This does not support the loss of alkalis into the host. Therefore, we conclude that the P-type MSI are virtually free from post-entrapment modification and represent original trapped melts. The plagioclase-enriched nature of the melt composition may be interpreted in terms of the fluid flux-induced dissolution of plagioclase as discussed above. The high-An rims of the plagioclase (Fig. 6c–e) are probably precipitates from the hydrous melt enriched in the plagioclase component as discussed by Hoshide & Obata (2009). The relationship between the P-type MSI and the high-An rims suggests that the plagioclase-enriched melt was trapped by the growing high-An rims.

Post-entrapment fractional crystallization of picritic melts in O-type MSI

While the picritic melt was entrapped in the growing olivines, the melt must have been saturated with olivine. Therefore, the first phase to precipitate from the trapped melt upon cooling would have been olivine. This newly precipitated olivine may become part of the olivine wall. This suggests that the entrapped melt must have been even more enriched in the olivine component. The absence of plagioclase in the O-type MSI indicates that the fractionated melt never became saturated with plagioclase. Instead, the occurrence of orthopyroxene in the MSI

Table 6: Representative microprobe analyses of mica and plagioclase

Ref. no.:	1	2	3	4	5	6	7	8	9	10	11	12	13	14	15	16
Mineral:	Asp	Bt	Asp	Bt	Bt	Asp	Bt	Bt	Bt	Bt	Bt	Asp	Bt	Plagioclase		
Zone:	AC							GR						chilled margin		
Sample:	92080901		92080912			91080507		91090708		92080701		92080706		LCM32		
Height (m):	7		21			36		62		66		71		0		
Type:	O-type	Matrix	O-type	O-type	Matrix	O-type	O-type	Matrix	Matrix	Matrix	Matrix	O-type	O-type	O′-type	O′-type	O′-type
Color:		b		g	b			b	b	b	b	b	g			
SiO_2	39·7	38·8	39·5	39·1	37·7	38·9	39·8	39·2	39·0	38·1	38·4	40·2	38·6	55·3	61·1	58·5
TiO_2	0·66	4·44	0·75	0·25	4·00	4·60	0·41	2·07	3·68	3·25	4·53	5·55	0·43	0·14	0·15	0·01
Al_2O_3	15·2	13·4	15·9	13·0	15·0	13·7	13·8	14·4	13·3	14·6	13·7	13·4	14·4	26·8	24·7	26·0
Cr_2O_3	0·11	0·25	0·02	0·01	0·02	0·05	0·00	n.a.	n.a.	0·00	0·01	0·00	0·02			
FeO	8·61	8·90	11·4	12·1	11·3	11·7	11·4	11·0	11·4	12·1	10·9	11·2	12·6	0·51	0·49	0·50
MnO	0·02	0·06	0·06	0·03	0·07	0·02	0·07	0·05	0·00	0·19	0·01	0·04	0·19	0·11	0·04	0·00
MgO	23·3	18·7	19·9	21·1	17·4	18·8	21·5	19·5	18·7	18·4	18·1	18·4	19·7	0·23	0·15	0·10
NiO	0·20	0·23	0·08	0·09	0·00	0·08	0·04	n.a.	n.a.	n.a.	n.a.	n.a.	n.a.	10·2	6·7	8·8
CaO	0·00	0·00	0·06	0·01	0·01	0·01	0·05	0·03	0·01	0·01	0·07	0·00	0·00	5·51	7·77	6·67
Na_2O	5·36	1·92	5·30	0·61	1·83	6·62	2·25	2·35	0·68	2·17	1·88	6·73	0·55	0·07	0·05	0·02
K_2O	0·77	6·87	1·21	6·98	7·66	0·39	5·22	6·70	8·98	6·61	7·51	0·37	7·30	98·9	101·2	100·7
F	0·07	0·05	0·01	0·00	0·04	0·00	0·00	n.a.	n.a.	0·06	0·25	0·00	0·00	*Formula based on 8 oxygen atoms*		
Cl	0·03	0·12	0·01	0·02	0·14	0·02	0·13	n.a.	n.a.	0·14	0·14	0·00	0·01	Si	2·52	2·69	2·61
Total	94·0	93·8	94·2	93·3	95·0	94·9	94·7	95·4	95·7	95·6	95·5	95·8	93·7	Ti	0·00	0·01	0·00
Formula based on 22 oxygen atoms														Al	1·44	1·28	1·36
Si	5·63	5·69	5·66	5·79	5·53	5·57	5·77	5·68	5·69	5·55	5·61	5·67	5·71	Fe	0·02	0·02	0·02
Ti	0·07	0·49	0·08	0·03	0·44	0·50	0·04	0·23	0·40	0·36	0·50	0·59	0·05	Mn	0·00	0·00	0·00
Al	2·53	2·32	2·68	2·28	2·59	2·32	2·36	2·46	2·28	2·51	2·35	2·22	2·52	Mg	0·02	0·01	0·01
Cr	0·01	0·03	0·00	0·00	0·00	0·01	0·00	n.a.	n.a.	0·00	0·00	0·00	0·00	Ca	0·50	0·32	0·42
Fe	1·02	1·09	1·37	1·50	1·38	1·40	1·38	1·34	1·39	1·48	1·33	1·32	1·56	Na	0·49	0·66	0·58
Mn	0·00	0·01	0·01	0·00	0·01	0·00	0·01	0·01	0·00	0·02	0·00	0·00	0·02	K	0·00	0·00	0·00
Mg	4·93	4·08	4·26	4·68	3·80	4·01	4·63	4·20	4·07	4·00	3·93	3·87	4·34	Total	5·00	4·99	5·00
Ni	0·02	0·03	0·01	0·01	0·00	0·01	0·00	n.a.	n.a.	n.a.	n.a.	n.a.	n.a.	An	50	32	42
Ca	0·00	0·00	0·01	0·00	0·00	0·00	0·01	0·01	0·00	0·00	0·01	0·00	0·00			
Na	1·47	0·55	1·47	0·17	0·52	1·84	0·63	0·66	0·19	0·61	0·53	1·84	0·16			
K	0·14	1·28	0·22	1·32	1·43	0·07	0·96	1·24	1·67	1·23	1·40	0·07	1·38			
Total	15·8	15·6	15·8	15·8	15·7	15·7	15·8	15·8	15·7	15·8	15·7	15·6	15·7			
F	0·03	0·02	0·01	0·00	0·02	0·00	0·00	n.a.	n.a.	0·03	0·12	0·00	0·00			
Cl	0·01	0·03	0·00	0·00	0·03	0·00	0·03	n.a.	n.a.	0·03	0·03	0·00	0·00			
OH	3·96	3·95	3·99	4·00	3·95	4·00	3·97	n.a.	n.a.	3·94	3·85	4·00	4·00			
Mg-no.	82·9	78·9	75·7	75·7	73·3	74·2	77·0	75·9	74·6	73·0	74·7	74·6	73·6			

Bt, biotite; Asp, aspidolite; b, brownish biotite; g, greenish biotite. Other abbreviations are the same as in Fig. 2.

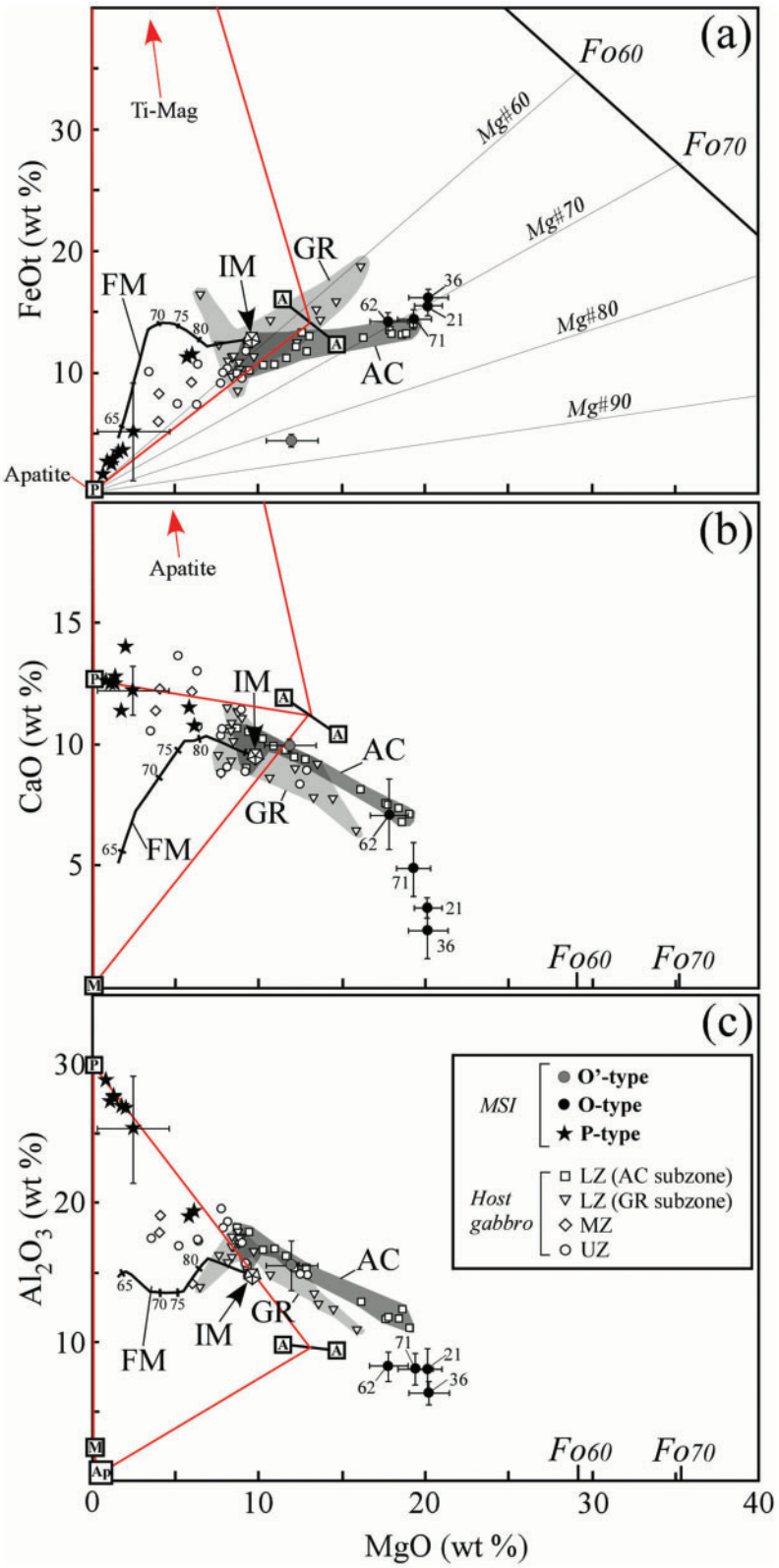

Fig. 13. Bulk compositions of MSI compared with the Murotomisaki whole-rock compositions. (a) MgO–FeO_t, (b) MgO–CaO and (c) MgO–Al_2O_3 diagrams. All data are plotted on an anhydrous 100% normalized basis. Numbers adjacent to the O-type MSI are the stratigraphic positions of the host-rocks. For P-type MSI, both the bulk composition of each inclusion and their average value (with 1σ) are shown. Whole-rock

(continued)

Table 7: Bulk compositions of MSI from the Muurotomisaki Gabbroic intrusion

Zone:	chilled margin		AC				GR						IM
Sample:	LCM32		91080912		91080507		91080708		92080706		91080509 and 92080706		
Height (m):	0		21		36		62		71		55 and 71		
Type:	O′-type		O-type		O-type		O-type		O-type		P-type		
n:	4	1σ	3	1σ	4	1σ	4	1σ	7	1σ	8	1σ	
SiO_2	52·19	1·11	46·80	1·55	47·55	0·86	46·12	1·10	47·08	1·46	48·64	2·98	48·83
TiO_2	1·17	0·33	0·72	0·12	1·89	0·27	1·98	0·40	2·08	0·55	0·84	0·92	1·17
Al_2O_3	15·47	1·76	7·99	1·55	6·32	0·84	8·36	1·04	8·04	1·16	24·93	3·91	14·98
FeO*	4·26	0·40	15·43	0·81	16·21	0·76	14·15	0·71	14·45	0·77	4·81	3·88	12·71
MnO	0·11	0·08	0·29	0·05	0·30	0·03	0·25	0·04	0·26	0·04	0·15	0·16	0·20
MgO	11·91	1·56	20·17	0·85	20·15	1·22	17·80	1·14	19·33	1·03	2·37	2·12	9·60
CaO	9·93	0·28	3·31	0·43	2·43	1·11	7·10	1·44	4·89	1·12	12·01	1·03	9·63
Na_2O	3·70	0·30	2·34	0·55	2·83	0·46	2·42	0·50	2·56	0·67	4·21	0·39	2·56
K_2O	0·16	0·04	0·30	0·09	0·13	0·01	0·07	0·03	0·10	0·04	0·12	0·09	0·22
P_2O_5											0·15	0·24	0·10
Total	98·90		97·38		97·84		98·25		98·79		98·14		100·00
mg-no.	83		70		69		69		70		47		57

*Total iron as FeO.
P-type MSI bulk compositions were obtained by SEM-EDS analysis. The O-type MSI from 21 m is Ti-poorer than the others because the aspidolite is Ti-poor owing to alteration (see Table A2). IM, initial melt (Akatsuka *et al.*, 1999) reported for comparison. Other mineral abbreviations are the same as in Fig. 2.

indicates that the fractionated melt had attained a reaction relationship with olivine:

$$\text{olivine} + \text{melt} = \text{orthopyroxene}. \quad (1)$$

Precipitation of anhydrous phases such as olivine and orthopyroxene in a chemically closed system, such as in the inclusion space, would lead to a concentration of H_2O in the residual melt and thus to an increase of the activity or the partial pressure of H_2O, which, in turn, should depress the plagioclase stability field (e.g. Yoder & Tilley, 1962; Holloway & Burnham, 1972; Helz, 1976). Recent experiments by Feig *et al.* (2006) and Botcharnikov *et al.* (2008), however, have shown that, even at high P_{H_2O}, plagioclase appears as a stable phase at relatively high temperatures [*c.* 1000°C at FMQ (fayalite–magnetite–quartz)] well before amphibole comes in (950°C at FMQ) in the crystallization of tholeiitic melts. This could be collateral evidence that a basaltic melt cannot be the parental melt of the O-type MSI. An inferred discontinuous reaction series deduced from the observation of the O-type MSI is orthopyroxene → clinopyroxene → amphibole → biotite (or aspidolite), which is well known as the calc-alkaline (or Bowen) trend, except for the appearance of aspidolite in the end. Inhibition of plagioclase crystallization would cause enrichment of Al and Na in the fractionated melts, and therefore, as fractionation advances, the pyroxenes would become aluminous and the amphibole Al- and Na-rich

Fig. 13 Continued
compositions of olivine gabbro from the AC and GR subzones are grouped and highlighted by dark and pale shading, respectively. A scale of olivine compositions is shown with a straight bold line in (a) and on the horizontal axes in (b) and (c). Straight fine lines represent isopleths of Mg-number. Curved bold lines represent the fractionation trend of the melt (FM) calculated using PELE (Boudreau, 1999*a*) for the Murotomisaki initial melt assuming 1 wt % H_2O, $P = 100$ MPa and $fO_2 = $ QFM buffer. Numbers on the fractionation trend represent the melt fraction. The initial melt composition (IM) is from Akatsuka *et al.* (1999). Approximate positions of amphibole (A), plagioclase (P), magnetite (M) and apatite (Ap) are indicated.

Table 8: The Fe–Mg exchange corrections applied to original bulk compositions of O′-type and O-type MSI

Zone:	chilled margin		GR subzone			IM
Sample:	LCM32		91080708			
Height (m):	0		62			
Type:	O′-type		O-type			
	original	Hypothetical melt	original	Hypothetical melt (a)	Hypothetical melt (b)	
100% normalized						
SiO_2	52·77	51·37	46·94	46·06	43·89	48·83
TiO_2	1·18	1·15	2·02	1·98	1·89	1·17
Al_2O_3	15·64	15·23	8·51	8·35	7·95	14·98
FeO*	4·31	10·27	14·40	18·37	28·27	12·71
MnO	0·11	0·10	0·25	0·25	0·24	0·20
MgO	12·04	8·31	18·12	15·40	8·63	9·60
CaO	10·04	9·77	7·23	7·10	6·76	9·63
Na_2O	3·74	3·64	2·46	2·41	2·30	2·56
K_2O	0·17	0·16	0·07	0·07	0·06	0·22
Total	100·00	100·00	100·00	100·00	100·00	99·90
mg-no.	83	59	69	60	35	57
Fo†		83		83	65	

*Total iron as FeO.
†Hypothetical olivine composition in equilibrium with bulk MSI as a melt. (See text for details.) Two results obtained assuming equilibrium olivines of Fo_{83} (a) and Fo_{65} (b) are listed for an O-type MSI.
IM, initial melt from Akatsuka *et al.* (1999).

(i.e. pargasitic). In the normal matrix outside the inclusion-bearing olivine, such an inhibition of plagioclase crystallization did not occur, probably because the parental melt for the normal matrix was an ordinary basaltic melt in contrast to that for the O-type MSI. Outside the olivine, therefore, the fractionation followed a different, normal tholeiitic trend. Judging from the locally developed orthopyroxene rims around olivine in the matrix (Fig. 3d), the fractionated melt may have eventually reached a reaction relationship with olivine in the matrix, and thereby orthopyroxene and hornblende precipitated interstitially; this stage would have been reached much later than in the MSI, after the saturation and substantial precipitation of plagioclase in the matrix. For this reason, Al enrichment did not occur in the pyroxenes and amphibole in the matrix.

The increase of the ferric–ferrous ratio from the core to the rim of the pargasite in the O-type MSI implies that progressive oxidation had taken place in the fractionated melts (Fig. 9). If H_2 diffuses out of the system (through the olivine host), as typically observed in nature (e.g. Herd *et al.*, 2002), the following H_2O dissociation reaction would proceed, consuming more H_2O and producing more oxygen in the melt, and thereby elevating P_{O_2} (Sato & Wright, 1966; Mathez, 1984):

$$H_2O \rightarrow H_2 + 1/2O_2. \quad (2)$$

Even if the fractionated melt became saturated with H_2O, P_{O_2} can still continue to be elevated as long as the loss of H_2 continued, by which process free water, even if it were once generated, may have been lost from the system by the time the melt became solidified. The increase of P_{O_2}, in turn, should cause an increase of the ferric–ferrous ratio in the melt (Botcharnikov *et al.*, 2005). The observed zoning of the MSI amphibole is, therefore, considered to provide evidence for such progressive oxidation that took place during the fractional crystallization of the MSI melts. The absence of ilmenite and the presence of titaniferous magnetite and hematite in the MSI is consistent with this scenario (see Fig. 3f; Buddington & Lindsley, 1964; Toplis & Carroll, 1995). It is important to emphasize here that the zoning of the amphibole, primarily generated during its growth, has been preserved despite the modification of the bulk composition via the Fe–Mg exchange reaction as discussed above.

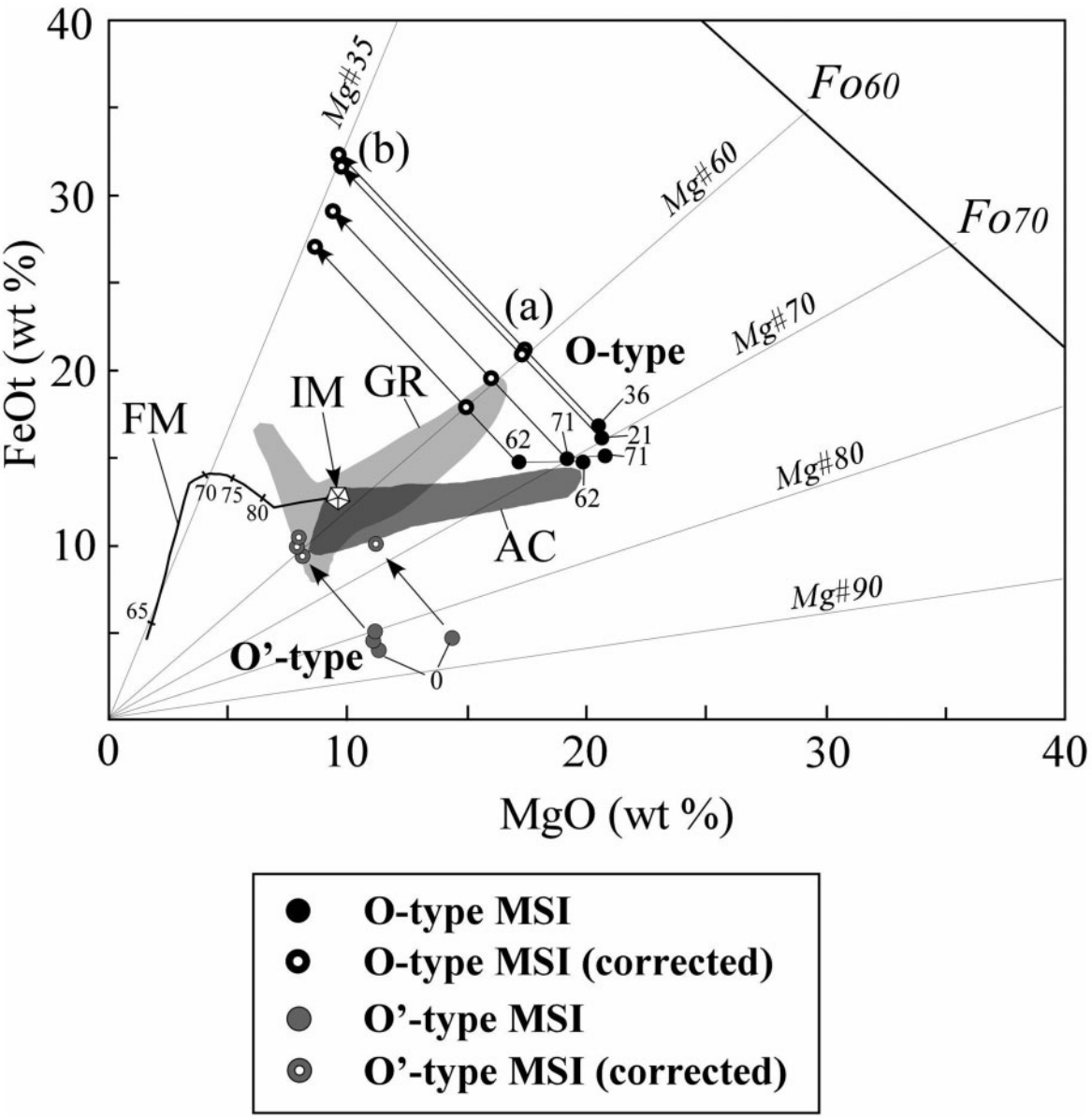

Fig. 14. The Fe–Mg exchange corrections applied to the bulk compositions of the O-type and O'-type MSI. The effects of the corrections are indicated by arrows. Two Mg-number values, 60 (a) and 35 (b), were assumed in the calculations for the O-type MSI. All Fe is assumed to be in ferrous state; FeO_t, total iron.

CONCLUSIONS

Important conclusions from this study may be summarized as follows.

(1) We recognize three types of amphibole-bearing multiphase solid inclusions (MSI) in silicate minerals from the Murotomisaki Gabbroic Intrusion: O- and O'-types in olivine and P-type in plagioclase. The bulk compositions of each type were obtained by microprobe and modal analyses.

(2) O'-type MSI that occur in phenocrystic olivines in the chilled margin most closely represent the trapped melts. Their composition is modified after entrapment by Fe–Mg exchange with the host olivine; the original melt entrapment must have occurred well before the magmatic emplacement.

(3) O-type MSI that occur in olivines are more enriched in the olivine component than O'-type MSI. They are interpreted to be crystallization products of hydrous picritic melts that were entrapped *in situ* by growing olivine crystals.

(4) Anomalous hydrous picritic melts were produced by dissolution of olivine when an H_2O-rich fluid

was introduced from a lower, more fractionated zone within the crystallization boundary layer.

(5) P-type MSI also represent trapped melts. Unlike the O-type MSI, they escaped post-entrapment Fe–Mg modification and were enriched in plagioclase components. Their anomalously high plagioclase content may also be ascribed to hydrous dissolution of plagioclase induced by H_2O-rich fluid introduction as in the case of olivine.

(6) It is proposed that a calc-alkaline fractionation trend occurred within O-type MSI where progressive increase of P_{H_2O} and P_{O_2} had occurred, as recorded in the growth zoning of the amphibole.

ACKNOWLEDGEMENTS

We thank T. Hirajima, T. Kawakami, M. Kitamura (Kyoto University), H. Sato (Kobe University), A. Toramaru (Kyushu University), S. Arai (Kanazawa University), and D. Spengler (Potsdam University) for their valuable discussions and comments at various stages of our research. We are particularly grateful to T. Kawakami for his technical assistance with electron microprobe analysis. Constructive reviews and criticisms by K. N. Pang and five anonymous reviewers were very helpful in improving the paper, and the editorial handling by C. W. Devey and M. Wilson is greatly appreciated.

FUNDING

T.H. acknowledges the Japan Society for the Promotion of Science for their financial support with a Grant-in-Aid for Research Fellow (No. 19.4363). This study was partially supported by a Grant-in-Aid for Scientific Research from Ministry of Education, Culture, Sports, Science and Technology (No. 21200052).

REFERENCES

Akatsuka, T., Obata, M. & Yokose, H. (1999). Formation of layered structure in the Murotomisaki gabbroic complex, especially picrite gabbro, Kochi Prefecture, Japan—Quantitative evaluation of crystal accumulation. *Journal of Geological Society of Japan* **105**, 771–788 (in Japanese with English abstract).

Anderson, A. T. (1973). The before-eruption water content of some high-alumina magmas. *Bulletin of Volcanology* **37**, 530–552.

Berry, A. J., Danyushevsky, L. V., O'Neill, H. S. C., Newville, M. & Sutton, S. R. (2008). Oxidation state of iron in komatiitic melt inclusions indicates hot Archaean mantle. *Nature* **455**, 960–963.

Botcharnikov, R. E., Al'meev, R. R., Koepke, J. & Holtz, F. (2008). Phase relations and liquid lines of descent in hydrous ferrobasalt—implications for the Skaergaard intrusion and Columbia River flood basalts. *Journal of Petrology* **49**, 1687–1727.

Botcharnikov, R. E., Koepke, J., Holtz, F., McCammon, C. & Wilke., M. (2005). The effect of water activity on the oxidation and structural state of Fe in a ferro-basaltic melt. *Geochimica et Cosmochimica Acta* **69**, 5071–5085.

Boudreau, A. E. (1999*a*). PELE—A version of the MELTS software program for the PC platform. *Computers and Geosciences* **25**, 21–203.

Boudreau, A. E. (1999*b*). Fluid fluxing of cumulates: the J-M reef and associated rocks of the Stillwater Complex, Montana. *Journal of Petrology* **40**, 755–772.

Buddington, A. F. & Lindsley, D. H. (1964). Iron–titanium oxide minerals and synthetic equivalents. *Journal of Petrology* **5**, 310–357.

Chen, Y. & Zhang, Y. (2008). Olivine dissolution in basaltic melt. *Geochimica et Cosmochimica Acta* **72**, 4756–4777.

Coogan, L. A., Hain, A., Stahi, S. & Chakraborty, S. (2005). Experimental determination of the diffusion coeffcient for calcium in olivine between 900°C and 1500°C. *Geochimica et Cosmochimica Acta* **69**, 3683–3694.

Danyushevsky, L. V., Della-Pasqua, F. N. & Sokolov, S. (2000). Re-equilibration of melt inclusions trapped by magnesian olivine phenocrysts from subduction-related magmas: petrological implications. *Contributions to Mineralogy and Petrology* **138**, 68–83.

Dixon, S. & Rutherford, M. J. (1979). Plagiogranite as late-stage immiscible liquids in ophiolite and mid-ocean ridge suites: An experimental study. *Earth and Planetary Science Letters* **45**, 45–60.

Feig, S. T., Koepke, J. & Snow, J. E. (2006). Effect of water on tholeiitic basalt phase equilibria: an experimental study under oxidizing conditions. *Contributions to Mineralogy and Petrology* **152**, 611–638.

Gaetani, G. A. & Watson, E. B. (2000). Open system behavior of olivine-hosted melt inclusions. *Earth and Planetary Science Letters* **183**, 27–41.

Hamamoto, R. & Sakai, H. (1987). Rb–Sr age of granophyre associated with the Muroto-misaki gabbroic complex. *Science Reports of the Faculty of Science, Kyushu University, Geology* **15**, 131–135 (in Japanese with English abstract).

Helz, R. T. (1976). Phase relations of basalts in their melting ranges at $PH_2O = 5$ kb, part II. Melt compositions. *Journal of Petrology* **17**, 139–193.

Herd, C. D. K., Borg, L. E., Jones, J. H. & Papike, J. J. (2002). Oxygen fugacity and geochemical variations in the martian basalts: Implications for martian basalt petrogenesis and the oxidation state of the upper mantle of Mars. *Geochimica et Cosmochimica Acta* **66**, 2025–2036.

Hofmann, A. W. (1980). Diffusion in natural silicate melts: a critical review. In: Hargraves, R. B. (ed.) *Physics of Magmatic Processes*. Princeton, NJ: Princeton University Press, pp. 385–417.

Holloway, J. R. & Burnham, C. W. (1972). Melting relations of basalt with equilibrium water pressure less than total pressure. *Journal of Petrology* **13**, 1–30.

Hoshide, T. & Obata, M. (2009). Zoning and resorption of plagioclase in a layered gabbro, as a petrographic indicator of magmatic differentiation. *Transactions of the Royal Society of Edinburgh: Earth Sciences* **100**, 235–249.

Hoshide, T., Obata, M. & Akatsuka, T. (2006). Crystal settling and crystal growth of olivine in the magmatic differentiation—the Murotomisaki Gabbroic Complex, Shikoku, Japan. *Journal of Mineralogical and Petrological Sciences* **101**, 223–239.

Jakobsen, J. K., Veksler, I. V., Tegner, C. & Brooks, C. K. (2005). Immiscible iron- and silica-rich melts in basalt petrogenesis documented in the Skaergaard intrusion. *Geology* **33**, 885–888.

Jakobsen, J. K., Veksler, I. V., Tegner, C. & Brooks, C. K. (2011). Crystallization of the Skaergaard intrusion from an emulsion of immiscible iron- and silica-rich liquids: evidence from melt inclusions in plagioclase. *Journal of Petrology* **52**, 345–373.

Kamenetsky, V. S., Crawford, A. J., Eggins, S. & Mühe, R. (1997). Phenocryst and melt inclusion chemistry of near-axis seamounts, Valu Fa Ridge, Lau Basin: insight into mantle wedge melting and

the addition of subduction components. *Earth and Planetary Science Letters* **151**, 205–223.

Leake, B. E., Woolley, A. R., Arps, C. E. S. *et al.* (1997). Nomenclature of amphiboles: report of the subcommittee on amphiboles of the International Mineralogical Association, commission on new minerals and mineral names. *Canadian Mineralogist* **35**, 219–237.

Li, C., Ripley, E. M., Sarkar, A., Shin, D. & Maier, W. D. (2005). Origin of phlogopite–orthopyroxene inclusions in chromites from the Merensky Reef of the Bushveld Complex, South Africa. *Contributions to Mineralogy and Petrology* **150**, 119–130.

Lowenstern, J. B. (2003). Melt inclusions come of age: Volatiles, volcanoes, and Sorby's legacy. *Developments in Volcanology* **5**, 1–21.

Mathez, E. A. (1984). Influence of degassing on oxidation states of basaltic magmas. *Nature* **310**, 371–375.

McBirney, A. R. (1987). Constitutional zone refining of layered intrusions. In: Parsons, I. (ed.) *Origins of Igneous Layering*. Boston, MA: D. Reidel, pp. 437–452.

McBirney, A. R. (1993). *Igneous Petrology*, 2nd edn. Jones and Bartlett: London, 508 p.

McBirney, A. R. & Nakamura, Y. (1974). Immiscibility in late-stage magmas of the Skaergaard intrusion. *Carnegie Institution of Washington Yearbook* **73**, 348–352.

Medard, E. & Grove, T. L. (2008). The effect of H_2O on the olivine liquidus of basaltic melts: experiments and thermodynamic models. *Contributions to Mineralogy and Petrology* **155**, 417–432.

Metrich, M. & Clocchiatti, R. (1989). Melt inclusion investigation of the volatile behaviour in historic alkali basaltic magmas of Etna. *Bulletin of Volcanology* **51**, 185–198.

Milman-Barris, M. S., Beckett, J. R., Baker, M. B., Hofmann, A. E., Morgan, Z., Crowley, M. R., Vielzeuf, D. & Stolper, E. (2008). Zoning of phosphorus in igneous olivine. *Contributions to Mineralogy and Petrology* **155**, 739–765.

Philpotts, A. R. (1982). Compositions of immiscible liquids in volcanic rocks. *Contributions to Mineralogy and Petrology* **80**, 201–218.

Renna, M. R. & Tribuzio, R. (2011). Olivine-rich troctolites from Ligurian ophiolites (Italy): evidence for impregnation of replacive mantle conduits by MORB-type melts. *Journal of Petrology* **52**, 1763–1790.

Roeder, P. L. & Emslie, R. F. (1970). Olivine–liquid equilibrium. *Contributions to Mineralogy and Petrology* **29**, 275–289.

Saito, G., Morishita, Y. & Shinohara, H. (2010). Magma plumbing system of the 2000 eruption of Miyakejima volcano, Japan, deduced from volatile and major component contents of olivine-hosted melt inclusions. *Journal of Geophysical Research* **115**, B11202.

Sato, M. & Wright, T. L. (1966). Oxygen fugacity directly measured in volcanic glasses. *Science* **153**, 1103–1105.

Schumacher, J. C. (1997). Appendix 2. The estimation of the proportion of ferric iron in the electron-microprobe analysis of amphiboles. *Canadian Mineralogist* **35**, 238–246.

Scowen, P. A. H., Roeder, P. L. & Helz, R. T. (1991). Reequilibration of chromite within Kilauea Iki lava lake, Hawaii. *Contributions to Mineralogy and Petrology* **107**, 8–20.

Sobolev, A. V. & Shimizu, N. (1993). Ultra-depleted primary melt included in an olivine from the Mid-Atlantic Ridge. *Nature* **363**, 151–154.

Spandler, C., Mavrogenes, J. & Arculus, R. (2005). Origin of chromitites in layered intrusions: Evidence from chromite-hosted melt inclusions from the Stillwater Complex. *Geology* **33**, 893–896.

Toplis, M. J. & Carroll, M. R. (1995). An experimental study of the influence of oxygen fugacity on Fe–Ti oxide stability, phase relations, and mineral–melt equilibria in ferro-basaltic systems. *Journal of Petrology* **36**, 1137–1170.

Trua, T., Clocchiatti, R., Schiano, P., Ottolini, L. & Marani, M. (2010). The heterogeneous nature of the Southern Tyrrhenian mantle: Evidence from olivine-hosted melt inclusions from back-arc magmas of the Marsili seamount. *Lithos* **118**, 1–16.

Veksler, I. V. (2006). Crystallized melt inclusions in gabbroic rocks. In: Webster, J. D. (ed.) *Melt Inclusions in Plutonic Rocks. Mineral Association of Canada Short Courses* **36**, 100–122.

Yajima, T. (1972). Petrochemistry of the Murotomisaki gabbroic complex. *Journal of the Japanese Association of Mineralogists, Petrologists and Economic Geologists* **67**, 247–261.

Yajima, T., Kajima, M. & Nagamura, Y. (1977). On the role of igneous activities in the tectonic movement, with special reference to the Muroto peninsula igneous zone. *Journal of Geological Society of Japan* **83**, 395–409.

Yoder, H. S. & Tilley, C. E. (1962). Origin of basalt magmas; an experimental study of natural and synthetic rock systems. *Journal of Petrology* **3**, 77–89.

APPENDIX

Table A1: Modal compositions of MSI from the Murotomisaki Gabbroic Intrusion

Height	Sample	MSI no.	Amp	Opx	Pl	Oth		
Chilled margin, O′-type								
0 m	LCM32	6	40	3	37	20		
		9	61	4	27	9		
		7	43	6	41	10		
		5	47	5	42	6		
		av.	48	4	37	11		
		1σ	8	1	6	5		
			Amp	Opx	Micas	Talc	Hem	Oth
AC, O-type								
21 m	91080912	1	27	25	19	21	8	0
		3	35	25	19	19	2	0
		4	37	31	32	0	0	0
		av.	33	27	23	14	3	0
		1σ	4	3	6	10	3	0
36 m	91080507	2	14	61	26	0	0	0
		ACI1	45	34	20	1	0	0
		ACI2	21	31	31	15	0	1
		ACI3	42	23	20	14	0	2
		av.	30	37	24	8	0	1
		1σ	13	14	5	7	0	1
GR, O-type								
62 m	91080708	p1	55	24	2	15	1	4
		p2-1	83	0	0	17	0	0
		p2-2	52	12	21	13	1	1
		p8	68	3	0	26	1	1
		av.	64	10	6	18	1	1
		1σ	12	9	9	5	0	2
71 m	92080706	2	24	56	11	6	0	2
		3	29	28	41	0	0	2
		4	57	27	6	8	0	2
		5	45	15	13	26	0	1
		6	44	22	24	10	0	0
		8	46	17	16	20	1	0
		10	38	28	23	11	0	1
		av.	41	27	19	12	0	1
		1σ	10	13	10	8	0	1

av., average value of modal compositions in the MSI. Oth, others. Oth in the O′-type MSI is composed almost entirely of voids. Oth in the O-type MSI includes apatite, sulphide and clinopyroxene. Oth was not considered for calculation of the MSI bulk composition. Other mineral abbreviations are the same as in Fig. 2.

Table A2: Mineral composition used for bulk composition calculations

Sample	Height	MSI no.	Mineral	Reference no.	SiO_2	TiO_2	Al_2O_3	Cr_2O_3	FeO	MnO	MgO	CaO	Na_2O	K_2O	Total	Density (g cm^{-3})
O′-type																
LCM32	0 m (chilled margin)	6 (Table A1)	Amp	Table 3, No. 1	46·4	1·73	10·7	n.a.	6·9	0·1	17·2	11·4	2·4	0·32	97·2	3·12
			Opx	Table 4, No. 1	55·0	0·38	2·9	n.a.	11·5	0·3	27·9	2·3	0·4	0·03	100·6	3·55
			Pl	Table 6, No. 14	55·3	0·14	26·8	n.a.	0·5	0·1	0·2	10·2	5·5	0·07	98·9	2·67
		9 (Table A1)	Amp		47·6	3·06	9·6	n.a.	6·2	0·1	17·5	11·4	2·2	0·35	97·9	3·12
			Opx	Table 4, No. 1	55·0	0·38	2·9	n.a.	11·5	0·3	27·9	2·3	0·4	0·03	100·6	3·55
			Pl	Table 6, No. 16	58·5	0·01	26·0	n.a.	0·5	0·0	0·1	8·8	6·7	0·02	100·7	2·67
		7 (Table A1)	Amp	Table 3, No. 2	49·0	1·72	9·1	n.a.	5·5	0·3	18·6	11·5	2·0	0·23	97·9	3·12
			Opx	Table 4, No. 1	55·0	0·38	2·9	n.a.	11·5	0·3	27·9	2·3	0·4	0·03	100·6	3·55
			Pl	Table 6, No. 15	61·1	0·15	24·7	n.a.	0·5	0·0	0·2	6·7	7·8	0·05	101·2	2·67
		4 (Table A1)	Amp		48·6	1·53	10·1	n.a.	5·6	0·0	18·7	11·4	2·2	0·17	98·2	3·12
			Opx	Table 4, No. 1	55·0	0·38	2·9	n.a.	11·5	0·3	27·9	2·3	0·4	0·03	100·6	3·55
			Pl	Table 6, No. 16	58·5	0·01	26·0	n.a.	0·5	0·0	0·1	8·8	6·7	0·02	100·7	2·67
O-type																
91080912	21 m		Amp	Table 3, No. 6	41·9	1·62	12·4	0·08	13·0	0·1	13·8	9·4	3·7	0·11	96·1	3·12
			Opx*	Table 4, Nos 6, 7	53·5	0·10	1·4	0·01	18·9	0·5	24·5	0·8	0·0	n.a.	99·8	3·55
			Mica	Table 6, No. 3	39·5	0·75	15·9	0·02	11·4	0·1	19·9	0·1	5·3	1·21	94·1	3·09
91080507	36 m		Amp	Table 3, No. 8	44·8	2·73	9·2	0·01	13·3	0·2	14·7	7·7	4·5	0·15	97·2	3·12
			Opx*	Table 4, No. 10, 11	53·3	0·10	1·1	0·03	20·1	0·5	24·1	0·4	0·0	n.a.	99·7	3·55
			Mica	Table 6, No. 6	38·9	4·60	13·7	0·05	11·7	0·0	18·8	0·0	6·6	0·39	94·8	3·09
91080708	62 m		Amp†	Fig. 9	43·2	2·58	11·2	n.a.	12·1	0·2	14·3	10·8	3·2	0·07	97·7	3·12
			Opx*	Table 4, Nos 14, 15	53·0	0·16	1·8	0·01	18·7	0·5	24·7	0·9	0·0	n.a.	99·8	3·55
			Mica‡	Table 6, No. 12	40·2	5·55	13·4	0·00	11·2	0·0	18·4	0·0	6·7	0·37	95·8	3·09
92080706	71 m		Amp†	Fig. 9	43·2	2·58	11·2	n.a.	12·1	0·2	14·3	10·8	3·2	0·07	97·7	3·12
			Opx*	Table 4, Nos 19, 20	54·0	0·04	2·5	0·03	18·3	0·5	24·8	1·0	0·0	0·00	101·2	3·55
			Mica‡	Table 6, No. 12	40·2	5·55	13·4	0·00	11·2	0·0	18·4	0·0	6·7	0·37	95·8	3·09

For O′-type MSI from sample LCM32, the bulk compositions of all four MSI were obtained for each and they were averaged to obtain analysis no. 1 in Table 7. For four samples of O-type MSI, each set of representative microprobe analysis listed was combined with the respective average modal compositions listed in Table A1. n.a., not analyzed. Amp, amphibole; Opx, orthopyroxene, Pl, plagioclase.
*Average composition for zoned orthopyroxenes.
†Average composition for zoned amphiboles (calculated from a line profile in Fig. 9) used for 62 and 71 m sample MSI.
‡Average aspidolite composition obtained from the 71 m sample was used for both 71 m and 62 m samples; the average composition of zoned amphibole obtained from the 62 m sample was used for both the 62 m and 71 m samples.

Table A3: A comparison of bulk MSI analyses for one P-type MSI, obtained by two methods

Sample:	a P-type MSI from sample 91080509 (55 m from the base)				
Phase:	Pl	Amp	Pum		
Mode (vol. %)	88	11·1	0·9		
Density (g cm^{-3})	2·67	3·12	3·20		
	Mineral analyses (wt %)			MSI bulk analyses	
	Pl	Amp	Pum	(1)	(2)
SiO_2	53·2	43·6	36·3	51·7	51·3
TiO_2	n.d.	2·24	n.d.	0·28	0·24
Al_2O_3	29·9	9·49	25·9	27·2	27·3
FeO*	0·45	17·1	6·87	2·63	2·86
MnO	n.d.	0·30	0·24	0·04	0·00
MgO	n.d.	11·3	0·44	1·44	1·25
CaO	12·8	11·1	22·9	12·6	12·8
Na_2O	4·35	2·27	n.d.	4·03	4·23
K_2O	0·08	0·27	n.d.	0·10	0·06
Total	100·7	97·6	92·7	100·0	100·0

*Total Fe as FeO.
n.d., not determined. Pum, pumpellyite. Minerals were analyzed with a WDS microprobe. (1), Method (1); that is, calculated from mineral and modal analyses. (2), Method (2); that is, direct raster-scan mode analyses using SEM-EDS. (See text.) Both bulk analyses are unhydrous 100% normalized.